Travail de fin d'études et stage[BR]- Travail de fin d'études : Optimization of E-fuels Production and Water Utilisation in Remote Renewable Energy Hub with Carbon Capture and Storage[BR]- Stage

Auteur : Swerdtfegers, Hugo
Promoteur(s) : Ernst, Damien
Faculté : Faculté des Sciences appliquées
Diplôme : Master en ingénieur civil électromécanicien, à finalité spécialisée en énergétique
Année académique : 2023-2024
URI/URL : http://hdl.handle.net/2268.2/19896

FACULTÉ DES SCIENCES APPLIQUÉES
Ecole d'ingénieurs et d'informaticiens

LIÈGE université

University of Liege
Faculty of Applied Sciences

Optimization of E-fuels Production and Water Utilisation in Remote Renewable Energy Hub with Carbon Capture and Storage

Master's thesis carried out to obtain the degree of
Master in Electromechanical Engineering by

SWERDTFEGERS Hugo

Supervised by
Ir. Dachet Victor
Prof. Ernst Damien

Academic Year 2023-2024

Contents

List of Figures

List of Tables

Abstract

This report explores the techno-economics of producing carbon-neutral synthetic fuel using Remote Renewable Energy Hubs (RREH). A RREH is a Power-to-X concept that aims to integrate and optimize renewable resources, designed in a remote area where high-quality renewable resources are abundant and harvested. The entire energy supply chain is modeled to characterize connectivity between technologies and processes.

The reference scenario considers the production of carbon-neutral synthetic methane, powered by solar and wind energy in Algeria, for delivery to North-western European market by 2030 for a system supplying 10 TWh annually.

The model has been developed to integrate Direct Ocean Capture (DOC), capturing carbon dioxide in the water rather than in the air. Results indicate a cost reduced by 2.94% for the DOC scenario. Sensitivity analysis considers various parameters, including investment costs and operational flexibility, revealing configurations lowering the price by 8.28%.

The study was then extended to account for the system's water output, by considering it as a by-product with potential utility for local communities. Findings illustrate a scenario in which water is priced at 3.09 €/t, equivalent to the one in Europe, facilitating the provision of fresh water to thousands of residents. Other more favorable configurations offer prices reduction of 9.1%.

A multi-hub configuration is then created to compare different hub locations economically and then see the possible interactions between them. The results show that a hub at Cap Horn, in southern Chile, can deliver synthetic methane at a cost reduced by 13.36% compared to the reference scenario.

Finally, the Fischer-Tropsch reaction is modeled to obtain synthetic fuels for decarbonizing the transport and aviation sectors (kerosene, diesel and gasoline). The implementation of several configurations suggests costs ranging from 2.41 €/kg to 2.13 €/kg, similar to those in the scientific literature. A techno-economic study shows optimistic prices reduces by 20.7% and the impact of a change in electrolyzer efficiency.

Acknowledgment

Realizing this work was really an incredible experience, this year was fantastic., especially thanks to a few people.

I would like to thank Prof. Damien Ernst for giving me the opportunity to do this TFE and the trust given. In particular, I would like to thank my supervisor Victor Dachet for all the support through the year. Being supervised in this way allowed me to feel comfortable throughout the year of work but also to improve greatly as a student.

Not working alone is always better, that's why I thank Antoine Larbanois, even if we didn't meet for long, but especially Gilles Ooms for the journey taken together, exchanging between us was always a pleasure. I thank also all the members of the Smart Grids Lab for their warm welcome.

And finally I would obviously like to thank all my friends, greatly thank my family and of course my girlfriend who spent this great year with me.

Chapter 1

Introduction

In these times where energy crises and environmental concerns continue to extend, designing optimized energy systems has become a major issue for the future. In recent years, the alarm has been sounded on excessive CO_2 emissions, while the demand for energy keeps rising [1]. The energy transition, especially through renewable energy sources, has thus begun in order to successfully reduce emissions despite the fact that their introduction includes a number of technical difficulties.

In order to help this transition and reduce CO_2 emissions, energy systems that incorporate concepts such as Power-To-X (PtX) [2] have been designated to reach a carbon-free energy system. This report illustrates this concept by designing and optimizing a remote renewable energy hubs (RREH).

An RREH is an energy hub located far away from large load centers where abundant, high-quality renewable energy is harvested [3]. Carbon-neutral fuels can be then produced to be used as primary materials in industry or used to generate electricity in external energy markets.

This thesis aims to develop the concept of RREH in mathematically modeled optimization frameworks of these energy systems. The "Graph Based Optimization Modelling Language" (GBOML) [4] developed at the University of Liège, will be used as a modelling tool to discuss the costs, storage, and efficiency of proposed optimized systems. The study will be based on the work of Mathias Berger's thesis [5], which studies the economy of carbon-neutral synthetic methane production from wind and solar resources in Algeria to supply Belgium's energy needs.

The first chapters will serve to contextualize the problem and introduce the concepts of PtX and RREH. The various equations, assumptions and elements required for simulations will also be discussed to set up the mathematical framework for the report.

To reach a carbon-free energy system, carbon dioxide is captured via Direct Air Capture (DAC) then combined with pure hydrogen to produce synthetic methane. Chapter 4 aims to introduce a new technology to replace DAC, namely Direct Ocean Capture. Since the marine ocean is a huge reservoir of CO2, it is possible to extract it using electrically powered membranes. The complete modeling of this recent but promising technology will be carried out by researching the techno-economic parameters of scientific studies. An economic report including sensitivity analyses and the study of technical parameters is made to compare the price of methane with the reference DAC scenario.

Chapter 5 examines the possibility of using water as a by-product of the RREH. While methane production requires a desalination plant, drinking water could also be produced to serve local regions in Algeria as well. To determine whether this is viable, the price of water per ton will be computed for several profiles and quantities of water supplied per day, but also by varying the techno-economic parameters of the desalination plant according to the conclusions reached in the literature review.

Chapter 6 will look at the creation of hubs in other interesting remote regions, in order to compare them economically and, more importantly, to see whether their joint integration would enable positive interactions between them.

While the production of other fuels such has ammonia or methanol has already been considered by Larbanois et al. [6], chapter 7 will introduce new ones. Here the products of the Fischer-Tropsch reaction are targeted, in particular gasoline, diesel and kerosene, which would make it possible to decarbonize the transport and aviation sectors. A complete modeling of the process will be completed to determine the cost of synthetic fuel as well as a sensitive analysis to consolidate the results.

Finally, Chapter 8 concludes the report and resumes the interesting outcomes of this research.

Chapter 2

Background

2.1 Renewable Energy Challenges

The challenges in the energy sector have been growing in recent years due to climate change, environmental concerns, and ever-increasing electricity demand. As the energy sector is responsible for 75% of European greenhouse gas emissions, the European Union has decided to set energy transition goals. For 2020, the aim was to reduce greenhouse gas emissions by at least 20%, increase the share of renewable energy (RE) to at least 20% of consumption, and make energy savings of 20% [7]. While the share of energy produced from renewable sources has been surpassed with a value of 22.1% [8], the initial target for 2030 to reach a proportion of 32.5% has been revised upwards with an intention to achieve a 45% share.

Many countries have therefore embarked on renewable energy transition policies. In 2020, Belgium consumed 85.6 TWh of electricity, with nearly 26% coming from renewable sources [9]. This is the result of a long evolution, given that in 2008 only 8.4% of electricity production came from renewable sources. While domestic renewable installations have been growing for several years (e.g., solar panels) as well as local energy developments (e.g., wind farms), the concept of RE giga-projects is relatively recent and represents an important field for research and development with the aim of significantly increasing the share of low-carbon sources in the energy mix.

2.2 Introduction to energy hubs

The majority of locations with great potential for RE are situated in remote and distant areas (for examples, the winds in Greenland [10] or the sun in North Africa [11]). This has led to the definition of a Remote Renewable Energy Hub (RREH), a center situated at a considerable distance from major load centers, where abundant and top-tier RE is harvested. The use of these resources would suggest the potential for a decarbonized system. Nevertheless, on a large scale, the technical challenge of renewable energies is to transmit electricity from where it is produced to where it will be consumed. This is a key element of the research and design currently underway. Indeed, it is imperative that projects are both energy-efficient and cost-effective. In order to attract investment, the system must demonstrate competitiveness in the market, with prices similar with current energy sources.

2.2.1 Renewable Systems Overview

The Three Gorges hydro-electric power plant in China, with 22.5 GW installed, making it the largest hydro-power installation in the world [12], harnesses the power of the river's water through turbines, generating electricity relatively consistently and usable in the surroundings of the station. Unfortunately, such projects are very rare due to the technical and geographical challenges associated with the massive infrastructure required around a river and its potential urban areas.

Therefore, various projects such as on/offshore wind farms are much more commonly used, like the Hornsea project, which employs wind turbines in the middle of the sea to capture marine winds 120 km off the coast of Yorkshire (UK) [13]. With 1 GW of installed capacity and 900 km of electrical cable, it supplies power to nearly 1 million homes (See Fig. 2.1). Although high-voltage direct current (HVDC) systems have seen significant development over time due to technical and structural improvements [14], direct transmission has its drawbacks. The lines must not be overloaded and do not have maximum efficiency including voltage sourced converter stations, resulting in losses from 1% to 3% depending on the transmitted power [15].

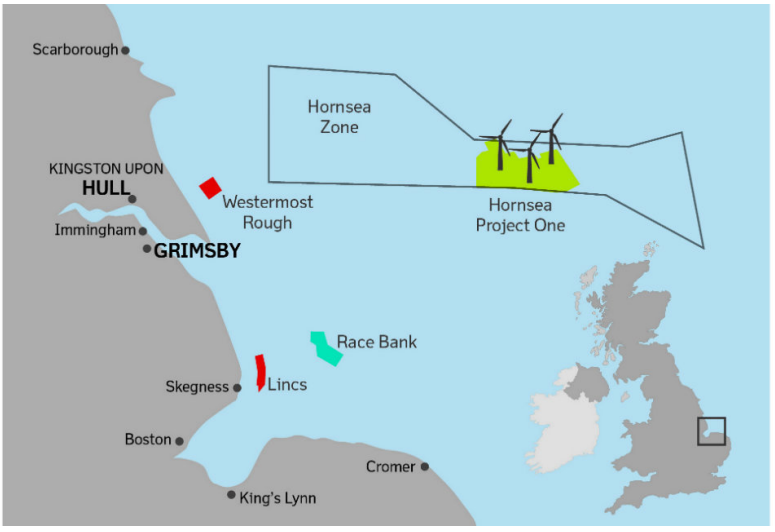

Figure 2.1: Illustration of the Hornsea project.

One significant constraint of such a system is that production is not always equal to demand. This has an even more substantial impact when the system is directly connected, in which case it is necessary to either curtail the wind turbines or install batteries in case of overproduction, or conversely, find another means of production when demand is too high.

To engage this issue, the concept of a global grid has been discussed in recent years, envisioning an electrical network connecting the entire world using a grid to collect renewable resources and distribute them efficiently. Green energy would arrive at stations that intelligently redistribute power through long, high-capacity lines. Research has already been conducted to develop this project [16], which aligns with the vision of a future with 100% RE production. The concept would effectively address the intermittency issue associated with most renewable sources, as countries could utilize the overproduction of distant nations (and vice versa). This would flatten demand and production curves by aggregating them into a single massive energy system, and the global grid can be seen as a set of connected hubs.

2.2.2 Power-to-X

Finally, the concept of power-to-x, still relatively new but very promising, involves the transportation of energy by molecules, either liquid or gaseous. Similar to how a battery works, electricity is used to produce a molecule that can either be used as raw material or converted back into electricity. Hydrogen serves as the backbone of this project, initially envisioned as a more efficient and cost-effective battery and more recently as a potential fuel.
Various studies have been conducted to determine which molecules are suitable for different applications in the power-to-x concept [17], each molecules with its own unique properties and advantages. These studies help identify the most appropriate molecules for energy storage, transport, or conversion, depending on specific needs and circumstances. To illustrate, hydrogen is a better way to store energy due to its high energy density, but it is challenging to transport compared to methane, which can be transported using existing gas infrastructure.

2.2.3 Remote hubs configuration

A RREH can utilize this power-to-x concept by producing large quantities of a molecule using abundant available renewable energy and then transporting it to places where its energy can be utilized. Fig. 2.2 represents the general operation of a hub.

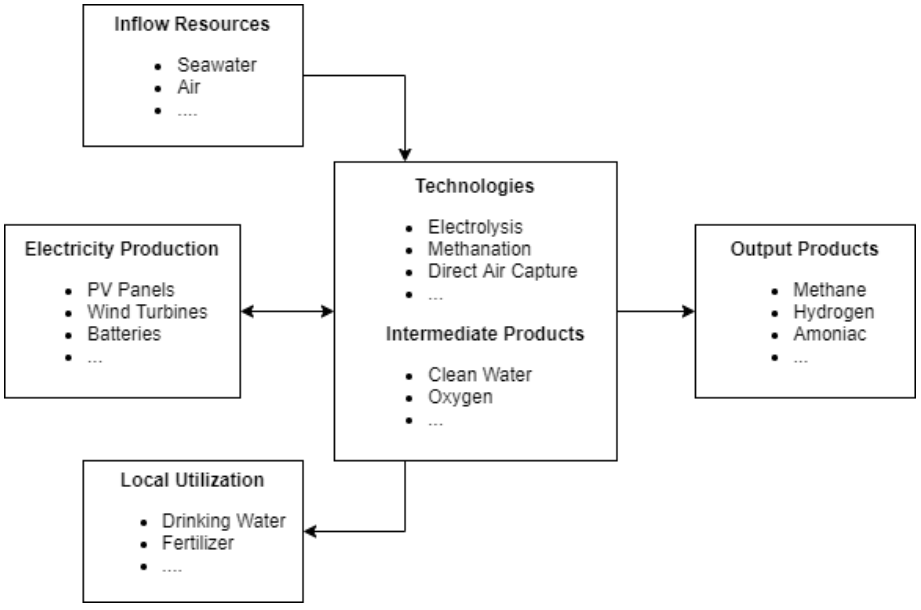

Figure 2.2: Schematic operation of a RREH.

The renewable energy sources, often solar panels and/or wind turbines, harness power at strategically chosen locations (c.f. 3.1). The generated electricity is then directly supplied to various technologies within the overall system. Batteries are in place to manage low-production periods. Backup generators running on natural gas can also be used, as seen in the study of Abdelshafy, A.M. et al. [18], which optimally designs a grid-connected desalination plant powered by RE resources.

Their study employs the basic concept of a remote hub with a single green energy-powered technology that produces water as the desired output, all within a limited boundary. However, the number of technologies involved can be substantial, with one technology possibly generating a valuable intermediate product for another, and the latter ultimately producing the desired final product. It is possible that some technologies may require the import of a freely accessible commodity (e.g., air) or a controlled one (such as stored CO2). Some may also generate by-products that could be locally valuable and developed in parallel with the initially sought product (e.g., drinking water), it can be seen as opportunities. Some hubs can produce multiple outputs, or they can be flexible and choose the desired molecule based on criteria like the external demand.

The synergy achieved through the integration of power-to-x principles with a RREH provides a versatile solution that adapts to the dynamic nature of energy needs, whether they involve raw materials or the conversion of electricity. This approach effectively mitigates the challenge of RE intermittency with a system offering a decarbonizing fuel while greatly benefit local communities.

2.3 Research context

The research carried out throughout this thesis is based on existing RREH models. To illustrate and introduce this concept, various studies will be presented such as the work of Mathias Berger with his study entitled *Remote Renewable Hubs for Carbon-Neutral Synthetic Fuel Production* [5] 2021, which will serve as a reference model.
His paper studies the economics of carbon-neutral synthetic fuel production where solar and wind energies needed are harvested in the Algerian desert, transported through a HVDC link where they are converted into carbon-neutral methane (CH_4) before being transported to Europe via shipping (see Fig. 2.3) to meet constant fictive demand equivalent to 10 TWh per year. A sensitivity analysis measure the impact of variations in techno-economic parameters or assumptions on the system's behavior, such as methane prices, different installed capacities, etc.

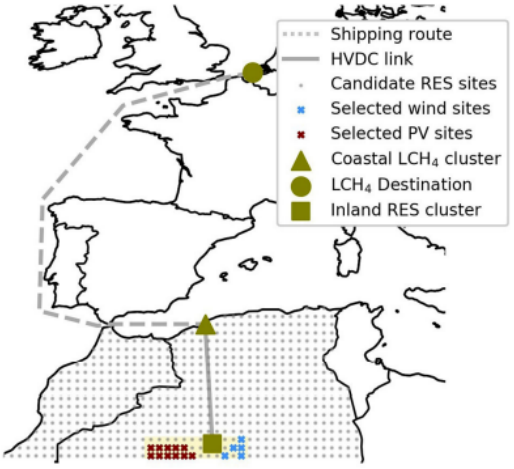

Figure 2.3: Remote carbon-neutral methane supply chain. Renewable energy is harvested in Algerian desert then transmitted to coastal cluster where LCH_4 is produced. The liquid fuel is then transported to Europe by ship.

Studies have already been carried out on the production of carbon-neutral fuel from renewable sources (Work on describing hydrogen costs by Chapman et al [19], 2017), but to model efficient and cost-effective systems, it is essential to account for all possible interactions between subsystems.

This can be seen as a remote renewable energy supply chain, a network composed of different components working together. To address the challenges related to this chain, it is essential to analyze these components together, understand how they interact in space and time, and gather sufficient technical details to represent their operations accurately (see Poncelet et al [20], 2016). This involves looking at the entire system, understanding how it is parts influence each other, and having precise information about their operation over time to make effective decisions.

Mathias Berger's study suggests a graph-based optimization modeling framework, where a hypergraph is temporally resolved incorporating on one side nodes representing a technology or process, each with its own optimization sub-problem containing their parameters, variables, constraints and objective functions, and on the other hyperedges representing the connectivity between different nodes to ensure the continuity of commodities passing from one node to another.

Fig. 2.4 shows the overall system diagram where each conversion or storage node is represented, linked by arrows connecting points symbolizing the hyperedges. The content within each node, whether input or output, can be identified using a color-coded system. The scheme is divided into distinct clusters, each representing parts of the system that correspond to different geographical areas. This division provides a more distinct understanding of the individual parts and their respective locations.

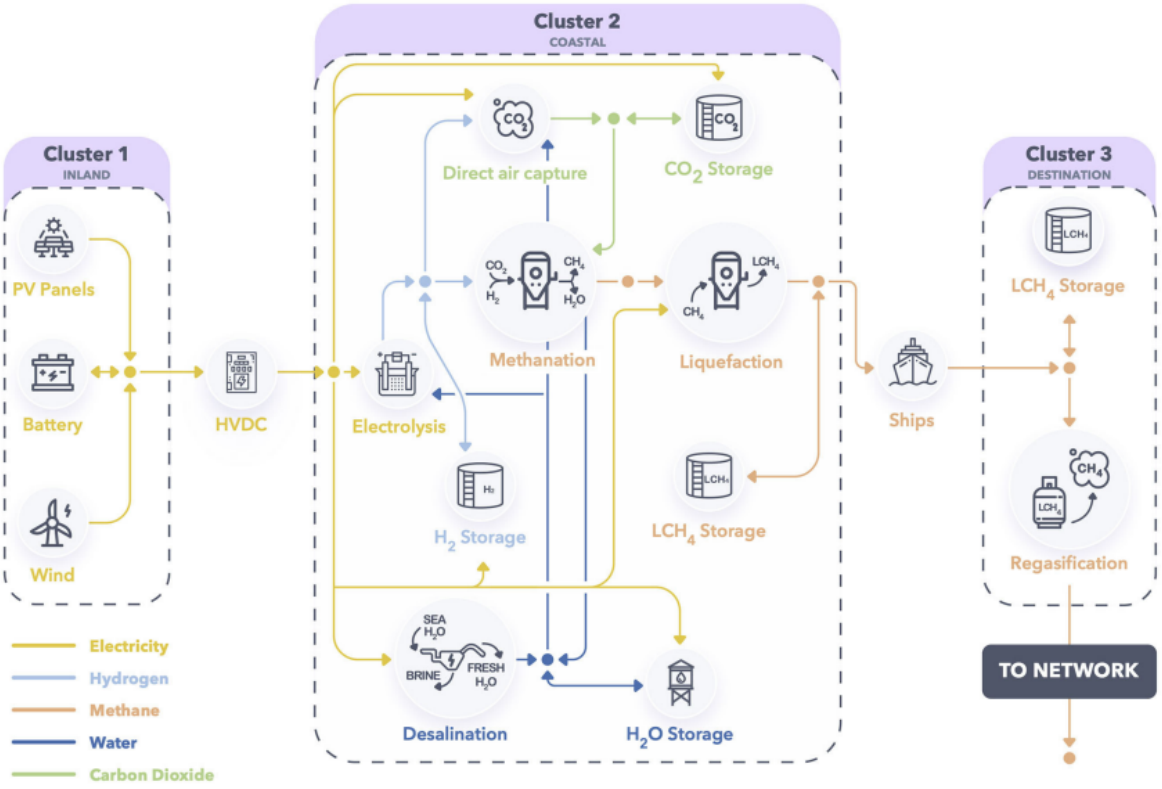

Figure 2.4: RREH configuration in Algeria from Bergel et al. [5]. Icons symbolize conversion or storage nodes, whereas bullets and arrows schematically denote conservation hyperedges.

The first cluster, representing electricity generation and storage, is located in central Algeria and is linked to the coastal cluster by HVDC where are situated all the processes needed to produce methane. In its liquid form, it is then transported to Europe by ship, fueling itself with the same methane and thus not using any fossil energy. Once the product reaches its destination, as the cluster name, it can then be either stored or used directly, either in its raw form or to generate electricity. The model is based on a constant demand of 10 TWh per year for a simulation period of 5 years.

The basic scenario, which will be used as a reference for the rest of this work, achieves a cost of synthetic methane at a higher heating value (HHV) of 149.7 €/MWh by 2030, providing 10 TWh each year, with a description of the system costs on Fig. 2.5.

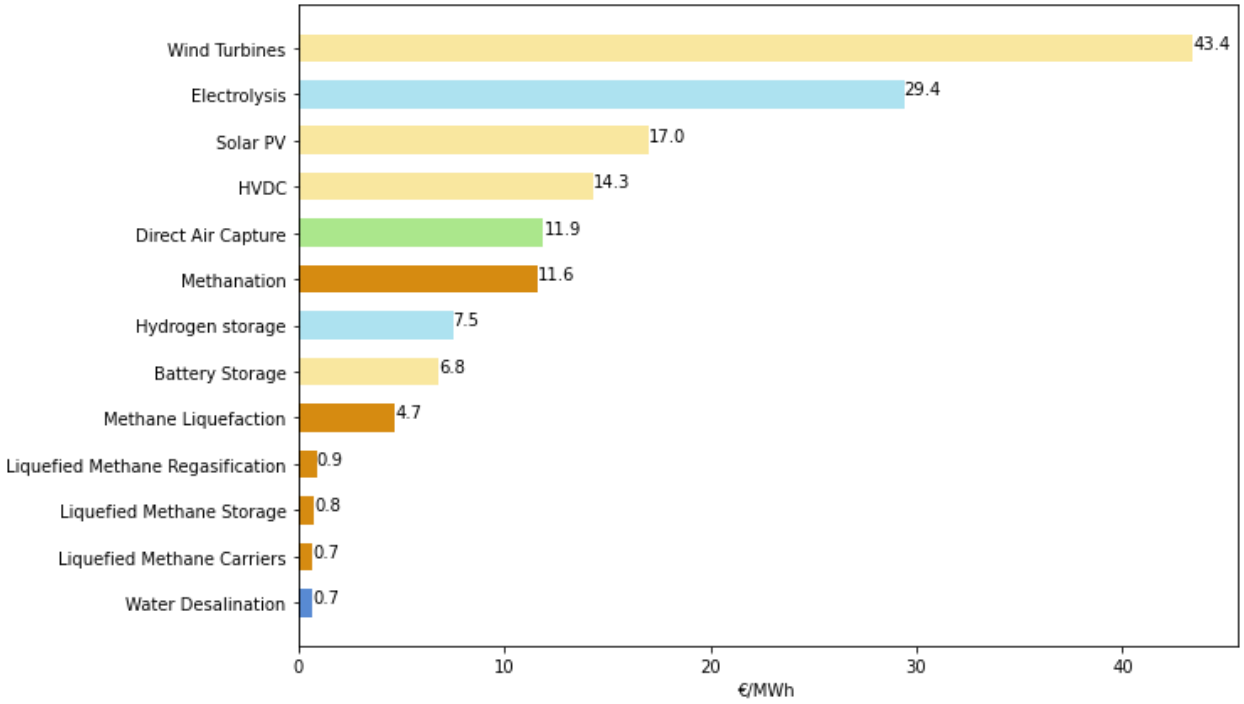

Figure 2.5: Cost Breakdown of Methane (HHV) for basic scenario with a total cost of 149.7 €/MWh from Berger et al. [5].

Each RREH presents different behaviors based on several parameters, such as the geographical area it utilizes, the technologies employed in the system, the desired output molecule, and more. The goal of each study is among others to optimize a proposed model in order to reduce the total system cost, attain realistic storage capacities, and/or identify the impact of changes in techno-economic parameters or configuration.
To illustrate, a study has been conducted on the various molecules that can be produced from the initial scenario [6], comparing not only their cost but also the technical and practical advantages and disadvantages.

	NH_3	CH_3OH	H_2	CH_4
Liquid	102	140	118	146
Gaseous	107	/	120	149

Table 2.1: Costs for different molecules in €/MWh
from RREHs from Larbanois A. et al. [6].

Based on the same scenario, the study *Towards CO2 valorization in a multi remote renewable energy hub framework* (by Dachet, V, et al [21]) is able to propose a total price of the system reduced by 9.2% by offering a multi-use of CO2 and multi-hub RREH. As well as being captured by the Direct Air Capture technology proposed earlier, CO2 could be harvested directly by PCCC (post-combustion carbon capture) in Belgian areas of high energy intensity. Furthermore, the study suggests using the wind energy potential in Greenland which has very advantageous characteristics [22] [23], in addition to the cluster in Algeria.

The results demonstrate a competitive price for the methane synthetic production using a multi-capture CO2 system . Reference prices to calibrate the European Emission Trading System are also proposed for the development of RREH.
Furthermore, the multi-hub approach highlights the qualities of each proposed region, including the quality of RE sources, available transportation/infrastructure, and local development opportunities.

This concept of a multi-hub approach aligns with the idea of a global grid, which involves establishing large-scale renewable energy production capacities. An emerging concept is to connect different hubs located in areas with high-quality energy resources, not only to optimize their individual systems but also to enable potential collaboration between them, favoring positive interactions to ensure that global energy demand is met with a maximum share of RE in the future.

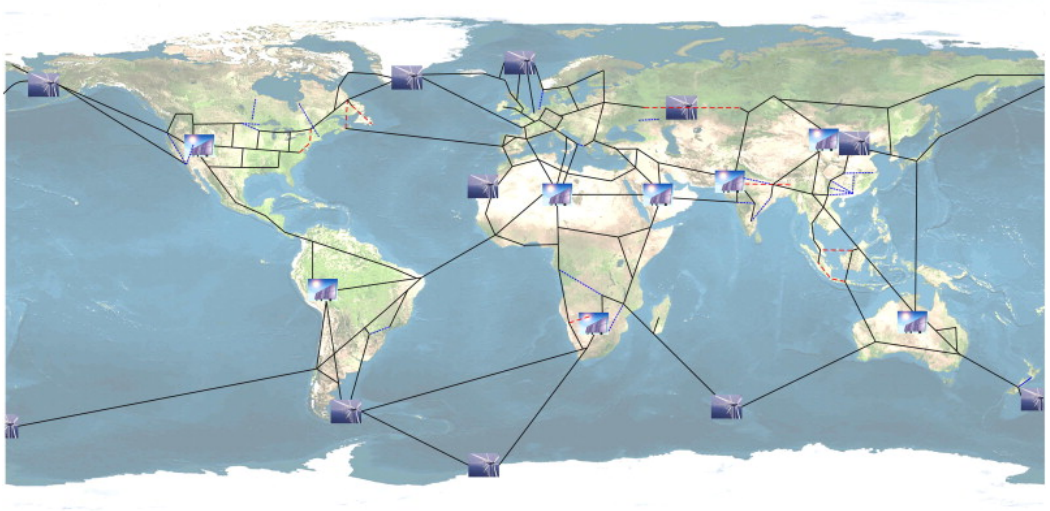

Figure 2.6: Illustration of the global grid concept [16].

Recently, TES, a worldwide green energy company, and the University of Liège successfully conducted their first joint research on the concept of RREH [24]. This collaboration holds the promise of accelerating the global transition to renewable and carbon-neutral energy.

The project, initiated in August 2023, aimed to assess the feasibility of producing carbon-neutral synthetic methane, or e-NG, in sunny regions of Morocco for use in Belgium [25]. The study modeled the energy supply chain to transport e-NG from Morocco to Belgium, examining three carbon dioxide acquisition systems, including DAC and PCCC. (See Fig. 2.7)

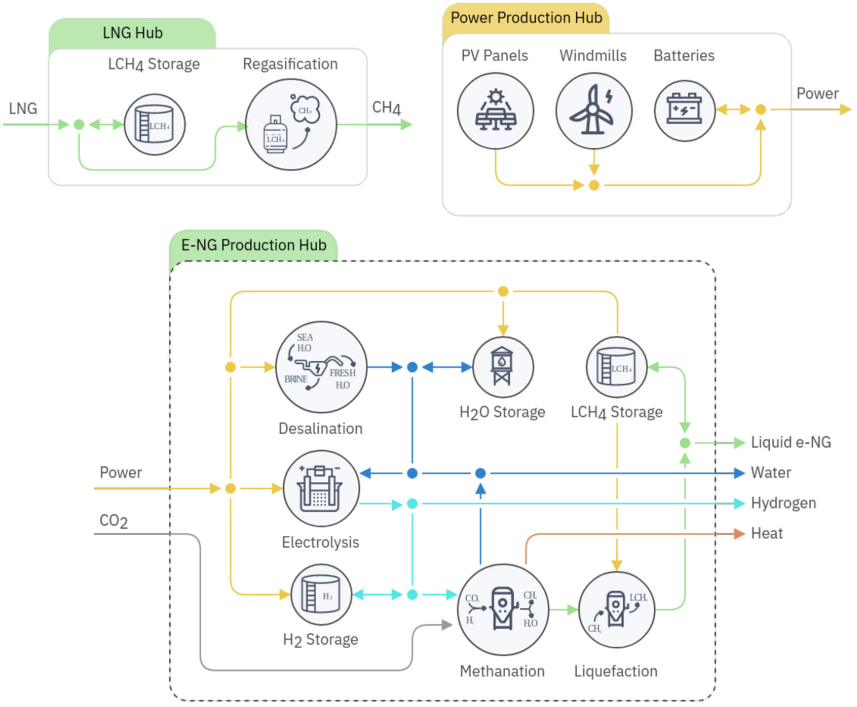

Figure 2.7: RREH configuration coming from *Synthetic methane for closing the carbon loop in Morocco* [25].

A key conclusion of the study highlights the effectiveness of PCCC for CO2 supply in e-NG synthesis, emphasizing the importance of existing infrastructure in the energy transition and aligning with the results obtained in the previous study on multi-hubs.

This introduction presents the challenges and foundations related to RREH and establishes the framework of the thesis, in order to examine more deeply the current challenges and opportunities. Their potential role in achieving energy sustainability goals is no longer in doubt, but the aim now is to optimize their design and operation to obtain efficient and competitive RREH.

2.4 Research objectives

This section aims to clearly define the fundamental objectives of this thesis to guide the work towards tangible and relevant results. The entire research is directed towards an in-depth understanding of the challenges related to RREHs and explores technical, operational, and economic aspects in detail to provide useful and pertinent information and conclusions.

First, a new method of carbon dioxide capture will be implemented with the introduction of Direct Ocean Capture (DOC), replacing the DAC in Mathias Berger's hub [5]. With this technology, CO2 can be extracted directly from the ocean water near the coast of Algeria and used in the coastal cluster. After providing an overview of this brand-new technology and implementing it, the impact of this replacement will be measured both in terms of the system's functionality and its economic aspects. A sensitivity analysis will be conducted on the techno-economic parameters of the DOC.

Next, a focus will be placed on a potential opportunity of the commodities in the initial scenario. Since Algeria is an arid region, develop fresh water production from the water desalination plant in the system can be worthwhile. After a complete review of the technology, data taken from studies will be used to create a hypothetical water demand to assess its impact on the system's operation and see the water costs to assess the demand.

Then several hubs will be created in selected regions with high renewable potential in order to be able to compare economically different RREHs. The final goal of this chapter will be to create a multi-hub, a model where multiple RREHs can provide multiple load centers.

The last chapter will focus on the creation of e-fuel to decarbonize the transport and aviation sectors. In particular, it will be gasoline, diesel and kerosene that will be created from the Fischer-Tropsch (FT) reaction where the process requires pure hydrogen and pure carbon dioxide, similar to methanation. After a brief description of the expected products, an economic analysis will be made to compare them with traditional fuels. After this will be done a technical analysis of the parameters of the new node created, the FT-process, in order to ensure the robustness of the results obtained.

All codes that were used to produce models and analyses in this report are available here.

Chapter 3

Methodology

This section is used to introduce the model and equations governing the behavior of the overall system, as well as the various concepts used throughout the analyses in the future sections.

3.1 GBOML Implementation

The system is modelled using GBOML (Graph-Based Optimization Modeling Language), a mathematical program created at the University of Liège [4] and used in applications from energy systems to supply chain. Implemented in Python, the program suits for structured mixed-integer linear problems solving the optimization in a discrete-time way over a finite time horizon T $\in \mathbf{N}$ with he set time of periods $\mathcal{T} = [0, 1, ..., T-1]$.

With the use of a block structure, each node n $\in \mathcal{N}$ contains its optimization sub-problem with $X^n \in \mathcal{X}^{\setminus}$ and $Z^n \in \mathcal{Z}^{\setminus}$ denote respectively the internal and coupling variables defined at node n. Each hyperedge in the set $\mathcal{E} \in 2^n$ ensures relations between them. Let denote F^n the local objective function for node n, with a scalar objectives of the form

$$F^n\left(X^n, Z^n\right) = f_0^n\left(X^n, Z^n\right) + \sum_{t \in \mathcal{T}} f^n\left(X^n, Z^n, t\right) \tag{3.1}$$

Finally, equality constraints with scalar functions h_k^n and inequality constraints with scalar functions g_k^n are defining on any hyperedge e $\in \mathcal{E}$ and involve the coupling variables of nodes incident at this hyperedge. The problem can then be written as a linear optimization that will be modeled as

$$\begin{aligned}
&\min \sum_{n \in \mathcal{N}} F^n\left(X^n, Z^n\right) \\
&\text{s.t. } h_k^n\left(X^n, Z^n, t\right) = 0, \forall t \in \mathcal{T}_k^n, k = 1, \ldots K^n, \forall n \in \mathcal{N} \\
&\quad g_k^n\left(X^n, Z^n, t\right) \leq 0, \forall t \in \overline{\mathcal{T}}_k^n, k = 1, \ldots \bar{K}^n, \forall n \in \mathcal{N} \\
&\quad H^e\left(Z^e\right) = 0, \forall e \in \mathcal{E} \\
&\quad G^e\left(Z^e\right) \leq 0, \forall e \in \mathcal{E} \\
&\quad X^n \in \mathcal{X}^n, Z^n \in \mathcal{Z}^n, \forall n \in \mathcal{N}.
\end{aligned} \tag{3.2}$$

3.1.1 Modelling Assumptions

The basic assumptions of the initial study [5] are re-used and described below

Centralized Planning and Execution: A single entity is responsible for both making investment decisions and operating the system. Its objective is to minimize the overall system costs.

Technology and Process Modeling: The sizing and operation of various technologies are represented using a set of linear input-output relationships. Typically, these expressions describe mass and energy balances at the plant or process level. Some technologies account for input or output dynamics, while storage technologies are represented in a simplified state space format.

Investment and Operational Strategy: This approach employs a static investment model, where investment choices are made at the start of the planning horizon, and assets are readily available. Operational decisions, on the other hand, are made on an hourly basis. Importantly, both investment and operational challenges are tackled simultaneously.

Predictive Capability and Knowledge: The entity in charge of system planning and operation possesses an exceptional level of foresight and knowledge. This means it can accurately predict future weather events, demand patterns, and has precise information about all technical and economic parameters, leaving no room for uncertainty.

3.1.2 Nodes

Conversion

Each conversion node n $\in \mathcal{N}$ processes a set of commodities i $\in \mathcal{L}^n$, external variables received as input or product as output (e.g., desalination plant has 2 commodities as it receives electricity to produce fresh water). The production of each commodity by a conversion node is governed by linear relations such as

$$q^n_{rt} - \phi^n_{ir} q^n_{i\left(t+\tau^n_i\right)} = 0, \forall i \in \mathcal{I}^n \backslash \{r\}, \forall t \in \mathcal{T}^n \tag{3.3}$$

where q^n_{rt} is the flow of commodity r at the time r, ϕ^n_{ir} is the conversion factor between commodity i and r and τ^n_i is the time of the conversion process.
The next equation arises from the static investment hypothesis, meaning that the capacity initially installed K^n_0 remains constant and does not change over the period T such as

$$K^n_0 - K^n_t = 0, \forall t \in \mathcal{T} \backslash \{0\} \tag{3.4}$$

where K^N_t is the capacity (K^N in the following). The total capacity therefore has as constraint

$$q^n_{r't} - \pi^n_t \left(\underline{\kappa}^n + K^n\right) \leq 0, \forall t \in \mathcal{T} \tag{3.5}$$

where $\underline{\kappa}^n$ represents the existing capacity. The availability parameter $\pi^n_t \in$ [0,1] represents the available capacity of a plant at time t. The capacity of a plant can also be bound such as

$$\left(\underline{\kappa}^n + K^n\right) - \bar{\kappa}^n \leq 0, \tag{3.6}$$

with $\bar{\kappa}^n$ the maximum capacity. The following equation represents an operational constraint, where the minimum operating level parameter $\mu \in [0,1]$ stands that the plant must have a minimum amount of commodities q_{it}^n in order to operate.

$$\mu^n \left(\underline{\kappa}^n + K^n\right) - \frac{\phi_i^n}{\phi_{r'}^n} q_{it}^n \leq 0, \forall t \in \mathcal{T} \tag{3.7}$$

The next equations, called ramping constraints, ensure that a certain continuity and logic are maintained. Flows can only be raised and lowered according to fraction of the installed capacity, with $\Delta_{i,-}^n$ and $\Delta_{i,+}^n \in [0,1]$

$$\frac{\phi_i^n}{\phi_{r'}^n} \left(q_{it}^n - q_{i(t-1)}^n\right) - \Delta_{i,+}^n \left(\underline{\kappa}^n + K^n\right) \leq 0, \forall t \in \mathcal{T} \backslash \{0\} \tag{3.8}$$

$$\frac{\phi_i^n}{\phi_{r'}^n} \left(q_{i(t-1)}^n - q_{it}^n\right) - \Delta_{i,-}^n \left(\underline{\kappa}^n + K^n\right) \leq 0, \forall t \in \mathcal{T} \backslash \{0\} \tag{3.9}$$

Finally, the objective function associated with each node n is defined as

$$F_n = v \left(\zeta^n + \theta_f^n\right) K^n + \sum_{t \in \mathcal{T}} \theta_{t,v}^n q_{r't}^n \delta t \tag{3.10}$$

where v is the number of years chosen to carry out the optimization, $\zeta^n \in \mathcal{R}_+$ is the CAPEX of a plant or in other words the investment cost which is annualised. Lastly θ_f^n and $\theta_{t,v}^n \in \mathcal{R}_+$ are respectively the fixed and variable operation and maintenance costs (FOM and VOM).

Storage

Each storage node n $\in \mathcal{N}$ hold only one commodity, although it can operate with an other one. In this context, every node possesses its own capacity, which is treated as an internal variable, while the external variables are the flows associated with charges and discharges.
Lets define i $\in \mathcal{L}$ and j $\in \mathcal{L}$ respectively the indices of inflows and outflows of the commodity and e_t^n the reserve level at time t, giving the basic equation of a storage node such as

$$e_{t+1}^n - \left(1 - \eta_S^n\right) e_t^n - \eta_+^n q_{it}^n + \frac{1}{\eta_-^n} q_{jt}^n = 0, \forall t \in \mathcal{T} \backslash \{T-1\} \tag{3.11}$$

where $\eta_-^n \in [0,1]$ is the discharge efficiency, $\eta_+^n \in$ the charge efficiency and $\eta_S^n \in$ the self-discharge parameter.

As mentioned earlier, storage nodes can operate with a commodity different from the one they store, denoted as q_{lt}^n with its conversion parameter ϕ_i^n (e.g., a water storage tank requires electricity to operate the pumps).

$$q_{lt}^n - \phi_i^n q_{it}^n = 0, \forall t \in \mathcal{T} \tag{3.12}$$

The next equation refers to the static investment assumption, given that the initial installed capacity is equivalent to that at the end of the time horizon such as

$$E_0^n - E_t^n = 0, \forall t \in \mathcal{T} \backslash \{0\} \tag{3.13}$$

where E_t^n is the total maximum capacity (E^n in the following). The relationship defining storage is thus

$$e_t^n - (\epsilon^n + E^n) \leq 0, \forall t \in \mathcal{T} \tag{3.14}$$

with ϵ^n the actual stock capacity. Operating rules must also be established, including the minimum inventory level required with the parameter $\sigma \in [0, 1]$.

$$\sigma^n (\epsilon^n + E^n) - e_t^n \leq 0, \forall t \in \mathcal{T} \tag{3.15}$$

The following two equations describe the behavior of flow capacity in relation to the installed capacity, with κ^n representing the existing flow capacity and $\rho^n \in \mathcal{R}_+$ denoting the maximum discharge-to-charge ratio, as in-outflows can have different maximum values.

$$q_{it}^n - (\kappa^n + K^n) \leq 0, \forall t \in \mathcal{T} \tag{3.16}$$

$$q_{jt}^n - \rho^n (\kappa^n + K^n) \leq 0, \forall t \in \mathcal{T} \tag{3.17}$$

Finally, the objective function associated with each node n is defined as

$$F_n = [v \left(\xi^n + \vartheta_f^n\right) E^n + \sum_{t \in \mathcal{T}} \vartheta_{t,v}^n e_t^n \delta t] + [v \left(\zeta^n + \theta_f^n\right) K^n + \sum_{t \in \mathcal{T}} \theta_{t,v}^n q_{it}^n \delta t] \tag{3.18}$$

where $\xi \in \mathcal{R}_+$ and $\zeta \in \mathcal{R}_+$ are respectively the stock and flow components of CAPEX, $\vartheta_f^n \in \mathcal{R}_+$ $\theta_f^n \in \mathcal{R}_+$ the stock and flow components of FOM and $\vartheta_{t,v}^n \in \mathcal{R}_+$ $\theta_{t,v}^n \in \mathcal{R}_+$ the stock and flow components of VOM.

Hyperedges

Each conservation hyperedge e $\in \mathcal{E}$ ensure local continuity between nodes exchanging the same commodity. Hence, every hyperedge has its associated commodity, and it is described that what exits must be equal to what enters. Let's define e_T and e_H as two subsets of nodes, and λ_t^e represents exogenous withdrawals or injections at every time t. The equation describing the equilibrium of each hyperedge is as follows

$$\sum_{n \in e_T} q_{it}^n - \sum_{n \in e_H} q_{it}^n - \lambda_t^e = 0\,, \forall t \in \mathcal{T} \tag{3.19}$$

3.2 Duality

In linear programming, duality is a concept that establishes a relationship between two linear problems. While the initial system being solved is called the primal problem, the dual problem is an alternative version used to find the optimal solution to the original problem. Below are illustrated the fundamental cases of the two associated linear systems.

Primal

$$\begin{aligned} \min \quad & c^T x \\ \text{s.t.} \quad & Ax \geq b \\ & x \geq 0 \end{aligned}$$

Dual

$$\begin{aligned} \max \quad & b^T y \\ \text{s.t.} \quad & A^T y \leq c \\ & y \geq 0 \end{aligned}$$

Duality has the advantage that when the optimal solution to the dual problem is achieved, it is also the optimal solution to the primal problem (and vice versa). The values of the optimal objective functions are also linked.

One relationship between the two problems is that dual variables are associated with a corresponding constraint from the primal problem. Each variables determine whether a constraint is restrictive (non-zero dual variable) or non-restrictive (zero dual variable).

Duality in linear programming serves as a powerful tool to assess the trade-off between resource constraints and costs in the context of energy optimization. The primal problem focuses on minimizing the cost function while satisfying resource constraints. In contrast, the dual problem seeks to maximize the value of the resources while adhering to certain cost limits. This duality principle allows us to examine the sensitivity of cost changes with respect to resource availability.

3.2.1 Dual Prices

In the context of a linear problem in energy domain, dual costs are the relative cost of a constraint associated with a resource, such as the cost of producing one additional unit of energy. So there is a different value for each constraint and for each time step t.

For example, if a dual value is 3, it means that increasing the production of 1 unit of the resource associated with the considered constraint will increase the cost by 3 units. The utility of these variables rest in the ability to quantify the possible variations in a constraint of the original problem, to determine whether a small change in production has a significant impact on the associated cost and indicate how this would affect the overall objective function of the problem.

3.3 Capacity Factors

In the energy sector, the Capacity Factor is an essential indicator for assessing the efficiency of an energy production facility. It measures the percentage of a facility's total capacity that is actually used to generate energy over a given period. It is calculated such as

$$\pi_t^n = \frac{\text{Real energy production}}{\text{Maximum theoretical production}} \times 100\% = \text{capacity factor of node n at time step t}$$

The higher the Capacity Factor, the more efficient the energy production facility is. A value of 100% means that the facility operates at full capacity all the time, while a lower one may indicate inefficiencies in the operation of the facility. This parameter is frequently used in the energy sector to assess the performance of installations such as wind turbines or PV panels.

The Capacity Factor is influenced by a variety of factors. Resource availability (such as wind for wind turbines or sunlight for solar panels), regular maintenance, and other operational factors can also affect it. This is why it is important to take it into consideration when optimizing investments related to RREH by identifying sites where conditions are most favorable for maximum production, ensuring reliable energy while minimizing costs.

To calculate the Capacity Factors of renewable installations, local meteorological data is essential. This data includes parameters like wind speed, pressure, sunlight, precipitation, and more. Using this information, mathematical models and simulation software are employed to estimate the expected energy production, accounting for the technical characteristics of the installation. The Capacity Factor is then calculated by comparing actual production to the theoretical maximum production.

3.4 DOC emplacement selection

Figure 3.1: Selected DOC installation site satisfying all technical criteria.

The choice of location for installing a new technology must be made based on its requirements while respecting real constraints, whether technological or societal. Assuming that the technology does not require excessively large space, it is nevertheless necessary for it to remain sufficiently in deep water while maintaining a reasonable distance from the coast and especially from the coastal cluster to ensure efficient transportation of outputs. The region outlined in red is considered a potential location, and the final choice is made arbitrarily marked by the red marker, at a distance equivalent to 50km from the coastal cluster.

Chapter 4

Direct Ocean Capture Plants

This chapter aims to introduce a new technology, namely the Direct Ocean Capture (DOC), and develop its modelization. Furthermore, its implementation within a RREH will be carried out by constructing its techno-economic parameters in a realistic manner.

4.1 Introduction and context

The overall operation of the DOC relies on electrically powered membranes, extracting carbon dioxide from seawater passing through them, and then sending the CO_2 through pipelines while releasing the water back into the ocean/sea.

The interest in this technology comes from the crucial role played by the ocean in absorbing carbon dioxide emissions from human activities, with nearly one third of emitted CO_2 being absorbed by the ocean. This makes the ocean the largest carbon reservoir on our planet. In fact, the concentration of CO_2 in the ocean is approximately 140 times greater than that in the atmosphere [26]. After processing on seawater, the water depleted of carbon dioxide is reintroduced into the ocean, enabling it to absorb additional CO_2 from the atmosphere.

While ocean CO2 extraction techniques were often based on biological methods such as microalgae cultivation, large-scale projects are based on electrochemical capture methods [27]. It is the case with the world's largest offshore carbon capture project, planned for Canada in 2024 [28]. Once operational and after successful testing, it aims to capture one million tonnes annually.

Figure 4.1: Large DOC project idealisation by Captura [29].

4.1.1 Overview of the technology

Although biological methods have been dominant for a while, electrochemical methods are proving to be more efficient and promising, especially due to better energy conversion factors as described by Jayarathna C. et al. (2022) [27], technologies that are however less scientifically documented. The article reviews recent advances in non-biological DOC technologies and mentions approaches such as ocean electrochemical capture, ocean alkalinity enhancement, mineralization, air stripping, and UV irradiation.

Among the electrochemical methods, one technology is considered promising due to its low electrochemical energy consumption and high capture efficiency, called bipolar membrane electrodialysis (BPMED) [30], which will be used for the implementation of DOC.

The process involves pushing the CO2/bicarbonate equilibrium toward dissolved CO2 by acidifying the ocean water. The acidified stream is then passed through a liquid-gas membrane contractor, which captures the gaseous CO2 from the dissolved CO2 in the aqueous stream.

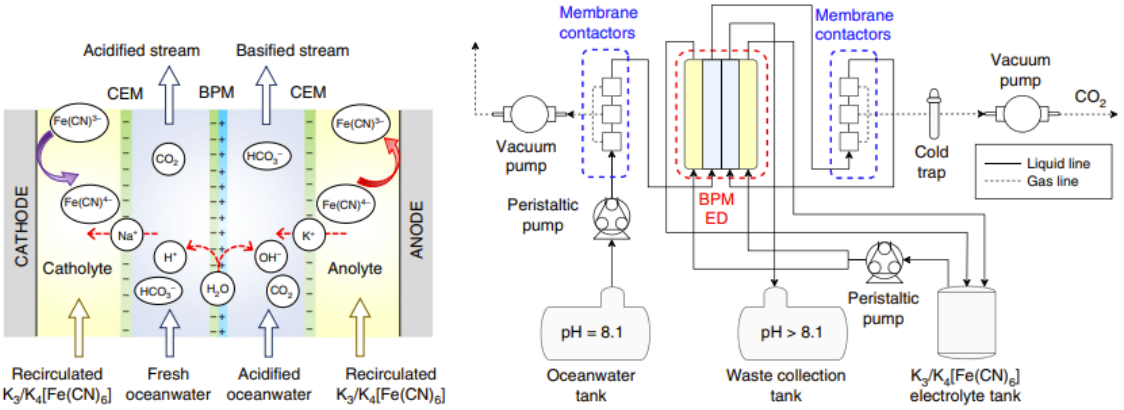

Figure 4.2: BPM electrodialysis cell on the left and CO2 capture system on the right showing a process flow diagram of the setup for CO2 capture from oceanwater [32].

The BPMED cell consists of two ocean water compartments separated by a bipolar membrane (BPM), two reversible redox-couple compartments separated by a cation exchange membrane (CEM), and two electrodes for electrochemical reactions. The BPM generates proton (H+) and hydroxide ion (OH-) fluxes via water dissociation reactions, converting the input ocean water into output streams of acidified and basified ocean water. The electrode solution contains a reversible redox-couple solution to minimize polarization losses.
A significant characteristic of this system is therefore its reliance solely on electricity as an input, which allows it to produce gaseous CO2 as an output.

Digdaya et al. (2020) [32] details the technology and lists the essential techno-economic parameters for modeling the DOC. The considered BPMED achieved an energy consumption of 151 kJ mol^{-1}, or 0.953 kWh kg^{-1} of CO2.
To test the robustness of the modeling, a sensitivity analysis will be conducted in Sec. 4.2.3 with the conversion factors from the studies of Eisaman et al. (2012) [30] and Yan et al. (2022) [31], corresponding to cases where consumption is higher or lower, respectively, with 1.528 kWh kg^{-1} and 0.663 kWh kg^{-1}.

4.2 Implementation and Simulations

Since the entire plant needs to be located at a certain distance from the coast, at the chosen site with optimal conditions (see Sec. 3.4), it is essential to model electricity and CO2 transmissions with, respectively, an HVDC and underwater pipelines, both of which incur non-negligible costs. This can thus be seen as the creation of a new cluster, called the marine cluster. Fig. 4.3 shows the integration of the new plant into the reference hub.

A significant difference lies in the fact that the DOC plant is not connected to the hydrogen and water hyperedges, unlike the DAC. The export to the network remains unchanged compared to the reference case, with a supply of 10 TWh per year.

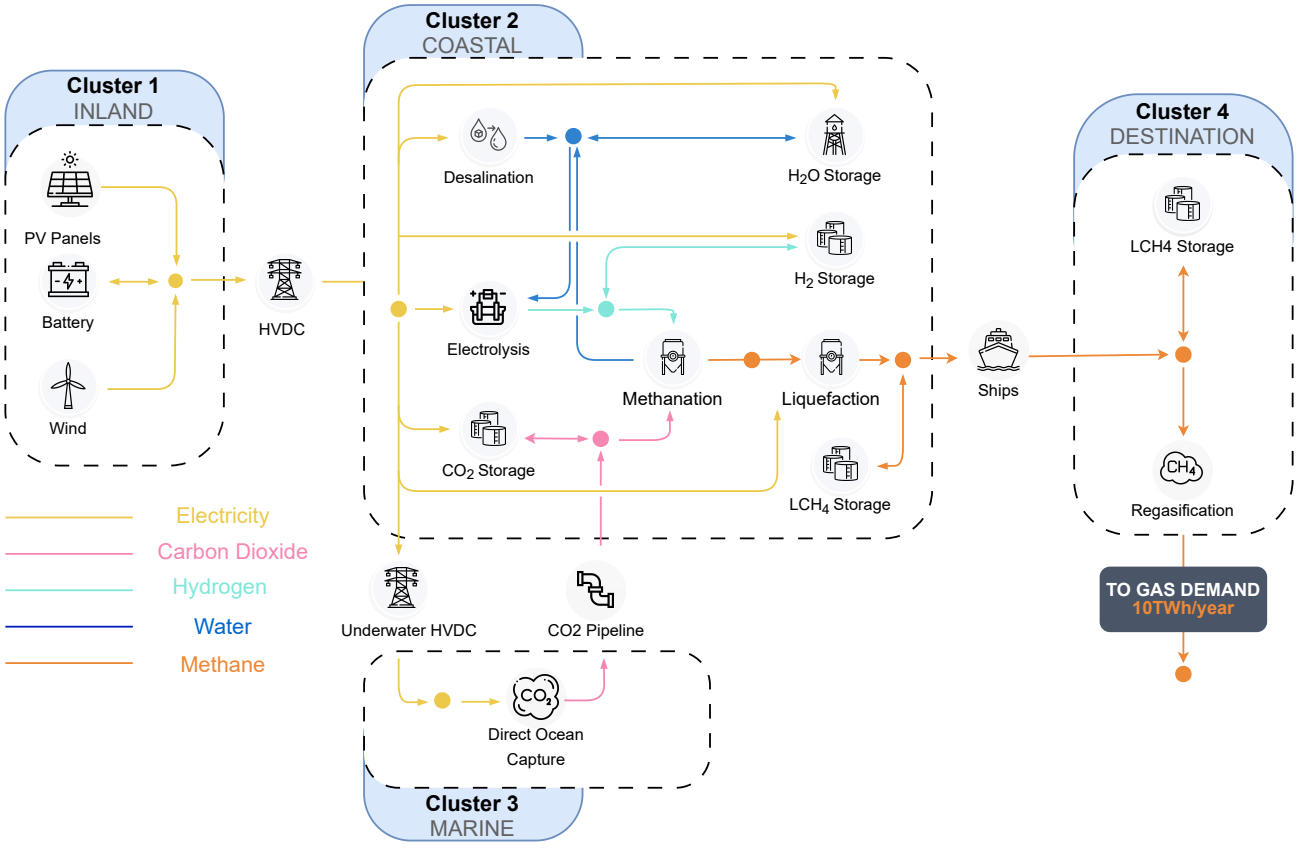

Figure 4.3: Remote hub system configuration adapted from Berger et al. [5] introducing DOC plant. Icons symbolize conversion or storage nodes, whereas bullets and arrows schematically denote conservation hyperedges.

The power is supplied through underwater HVDC cables, while the CO2 is transported back to the coastal cluster via an underwater pipeline. Both transportation methods are well-established technologies and can be readily implemented. Moreover, it is crucial to ensure that the system is located at a sufficient distance from the coast to provide the required depth without interfering with coastal human activities or marine transport. In this study, the suitable location for the system has a distance of 50km from the coast.

4.2.1 Techno-economical parameters

Selecting the parameters accurately is a significant challenge, especially to strike a balance between overly optimistic and overly pessimistic values. The techno-economic parameters have all been introduced in Sec. 4.1.1 and are drawn from studies, sometimes American. Therefore, the conversion of currency from dollars to euros will be considered with the exchange rate of May 1, 2023.

The chosen parameters for the DOC will be based on the findings of the scientific studies proposed by Digdaya, Ibadillah A., et al., (2020) [32] [33] who are more deeply interested in BPMED technology. The ability to model the direct ocean capture process with electricity as the only input is made possible by incorporating membrane replacement costs into FOM expenses.

Although the underwater HVDC employs the same technology as one installed on land, certain parameters differ and can be found in the study by Xiaoling Zhao, et al., 2020 [34]. This includes economic parameters, which are computed based on the total length of the HVDC, that increase due to additional installation constraints.

The pipelines transporting CO2 are modeled in a very traditional way, with maximum efficiency, and economic parameters calculated based on the total length. All the techno-economic parameters of the new nodes are listed in Tabs 4.1 and 4.2.

	CAPEX	FOM(θ_f)	VOM(θ_v)	Lifetime
Direct Ocean Capture	3160.8 M€/(ktCO2 /h)	0.09 M€/(ktCO2 /h)-yr	0.0738 M€/ktCO2	30 yr
CO_2 Pipeline (50km)	200 M€/(ktCO2 /h)	0.02 M€/(ktCO2 /h)-yr	0 M€/ktCO2	50 yr
Underwater HVDC (50km)	47.5 M€/GW_{el}	0.72 M€/$GW_{el} - yr$	0.0 M€/GW_{el}	30 yr

Table 4.1: Economical Parameters of nodes linked to DOC.

	ϕ_1	μ	$\Delta_{+,-}$
Direct Ocean Capture	0.953 GWh/ktCO2	1 -	0 -/h
CO_2 Pipeline (50km)	1 -		
Underwater HVDC (50km)	0.9499 -		

Table 4.2: Technical Parameters of nodes linked to DOC.

4.2.2 First results

In order to see whether the proposed system is viable, it is useful to compare the total costs to the original hub with DAC. By integrating the direct ocean capture into the remote hub, the cost of producing synthetic methane would decrease to 145.3 €/MWh for a system supplying 10 TWh annually. Fig. 4.4 shows the breakdown of costs by segment.

The main differences are located on the one hand in the part related to carbon dioxide and on the other hand in the division related to electricity production, with PV panels and wind turbines.

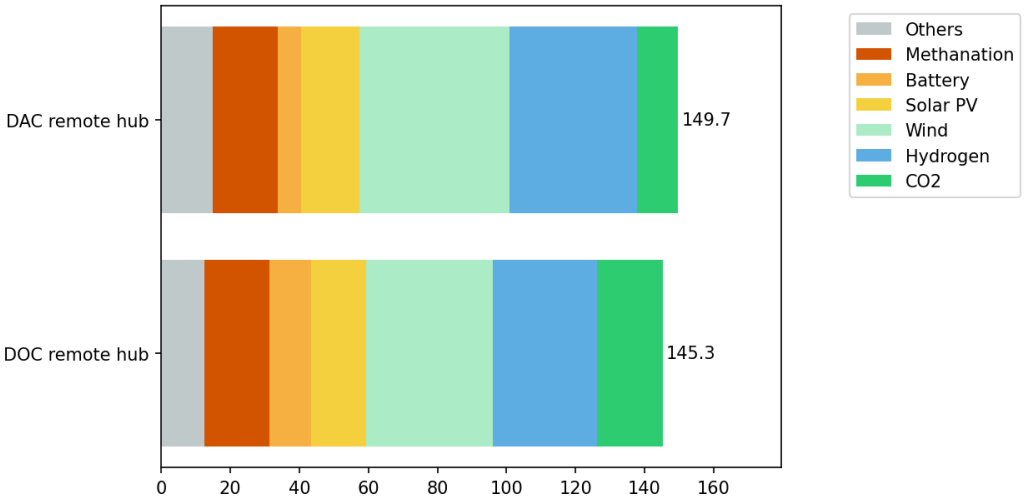

Figure 4.4: Cost Breakdown Comparison between DAC and DOC scenarios [€/MWh].

The higher cost of CO2 is due to the higher electricity consumption to absorb carbon dioxide in the ocean than in the air. Indeed, the consumption to have a ton of CO2 is 0.109 MWh for the DAC while the DOC consumes 0.953 MWh for that same quantity. However, the great force of capture in the ocean is the fact that the system does not need desalinated water or hydrogen input, unlike DAC. This makes it possible to reduce the electrolysis capacity from 3.1 to 2.3 GW_{el}.

This decrease in hydrogen production allows the system to consume less electricity given the significant conversion factor of 50.6 GWh/kt_{H2} for the electrolysis plant (See App. A.1). This is reflected by the fact that the capacity of the HVDC lines is reduced from 3.32 GW to 2.69 GW, and especially by the decrease of the renewable units capacities as shown in Fig. 4.5.

Unfortunately, despite the total electricity needs being reduced, the fact that the consumption of the node capturing CO2 increases means that the total installation capacity of batteries is increased, due to the inflexibility of the DOC, which operates constantly. 5.03 GWh of batteries significantly increases costs, further reinforcing doubts about such a total installed capacity.

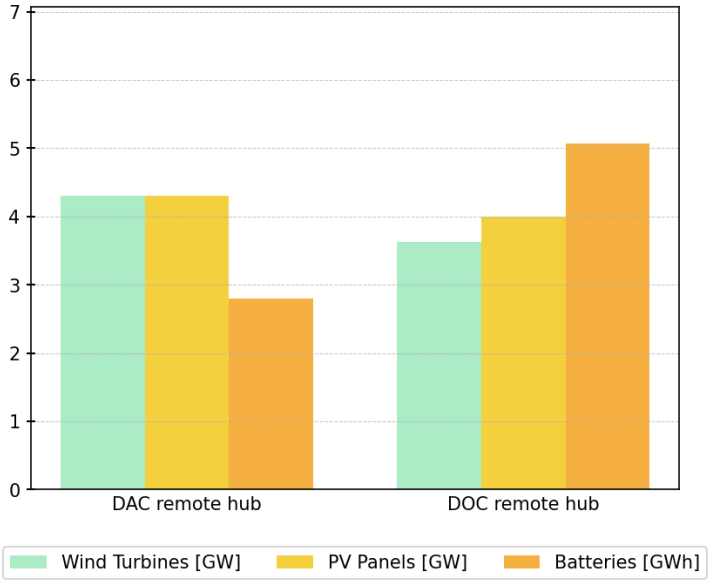

Figure 4.5: Capacities comparison between scenarios, with a decrease in power generations for DOC scenario trade-off by a increase in battery capacity.

An interesting change is the capacity of the water desalination unit which decrease from 1.3 kt/h to 0.17 kt/h. The vast majority of the desalinated water was used as direct air capture input, while it is no longer used only for electrolysis here, which has also been reduced in use.

Total costs are therefore reduced mainly because DOC only requires electricity as input. Despite its higher electricity consumption, this makes it possible to reduce the production of hydrogen and desalinated water, previously used to capture CO2, and therefore reduce the total electricity consumption, allowing the system to install less renewable production capacity.

4.2.3 Sensitivity Analysis

It is imperative to be cautious when considering the techno-economic parameters, particularly due to the technology's current lack of commercial maturity. Conducting a sensitivity analysis enables the evaluation of the ramifications of data adjustments, encompassing both optimistic and pessimistic scenarios. Tab. 4.3 resumes the different values used for each scenario.

	Optimistic	Reference	Conservative
CAPEX M€/(ktCO2 /h)	2528.6	3160.8	3792.9
VOM M€/ktCO2	0.05904	0.0738	0.08856
ϕ_1 GWh/ktCO2	0.663	0.953	1.528

Table 4.3: Variations of techno-economic parameters resulting in 3 scenarios compared in the sensitivity analysis.

While optimistic values may come from technological advancements or widespread commercialization, conservative values would reflect installation and usage difficulties, increasing costs and reducing efficiency. While the CAPEX/VOM will be increased and decreased by +20% and -20% respectively, values selected due to expertise accumulated during research, conversion values are adjusted based on various studies from literature review with values mentioned in Sec. 4.1.1. The results are shown in Fig. 4.6.

It logically appears that the only parts of the total cost impacted are those related to carbon dioxide production, namely everything concerning electricity generation and the DOC node itself. The amount of CO2 required remains the same to meet constant demand, but the amount of energy required to extract it varies, thus affecting the installed capacities of PV panels and wind turbines.

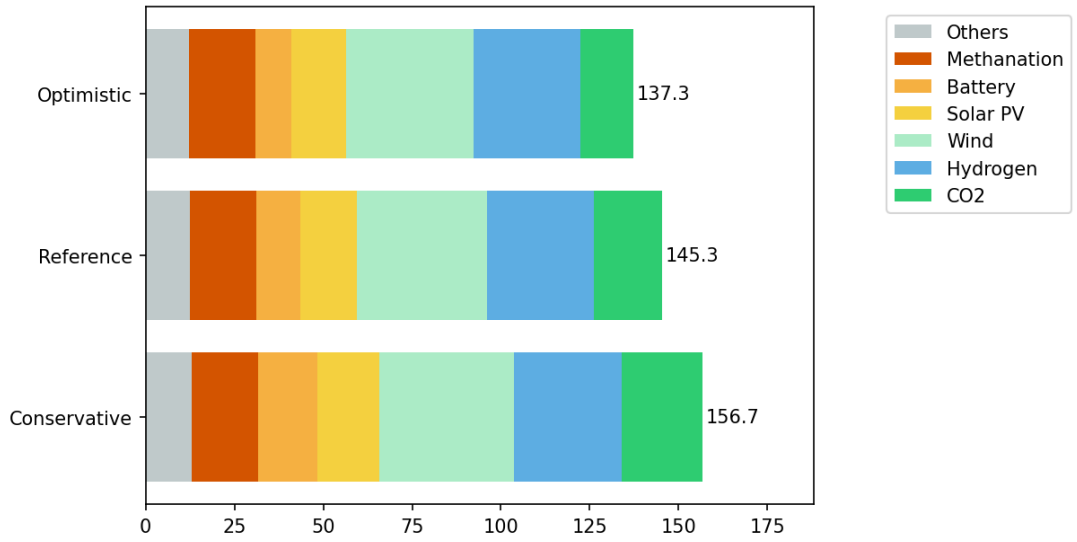

Figure 4.6: Cost Breakdown Comparison for reference, optimistic or conservative scenarios [€/MWh].

The optimistic scenario confirms the economic advantages of DOC over DAC by significantly reducing the total system cost. However, it is important to keep in mind that technological advancements may also occur for DAC technology, reducing either conversion factors or prices in the case of widespread commercialization. Monitoring the evolution of both technologies in parallel is interesting in order to reduce costs.. In the conservative scenario, the total system cost is higher than the reference case with DAC. One of the direct causes is the increase in installed battery capacity, from 3.58 GWh for the reference case to 5.03 GWh for this scenario.

If both the CAPEX/OPEX and the conversion factor of DOC were increased by 9.8%, the total cost would fall back to the value of the hub with DAC, at 149.7 €/MWh. The advantage of the solo input is also reflected here when conversion factors may differ from theory, increasing costs related to only one commodity (installed capacity/utilization/storage).

4.2.4 Variable DOC Operation

The purpose of this section is to assess the impact of a modeling change on the DOC. Due to mechanical constraints, it is modeled with the minimum level parameter set to 1 (see Eq. 3.7) which claims a maximum output quantity from the DOC technology continuously equals to his capacity. Based on the analyses conducted on the initial results, it is evident that attempting to operate it variably would optimize the system. Therefore, the following simulations will be conducted with $\mu = 0.5$. Results are displayed in Fig. 4.7.

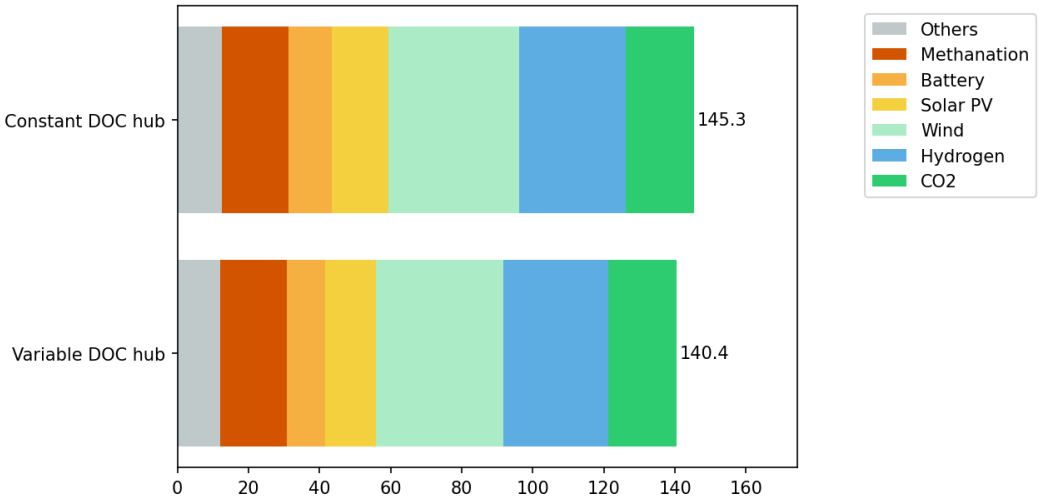

Figure 4.7: Cost Breakdown Comparison between constant or variable DOC operation [€/MWh].

The total cost is reduced significantly, mainly coming from the decrease in costs related to energy production. Fig. 4.8 clearly shows the causes of theses decreases.

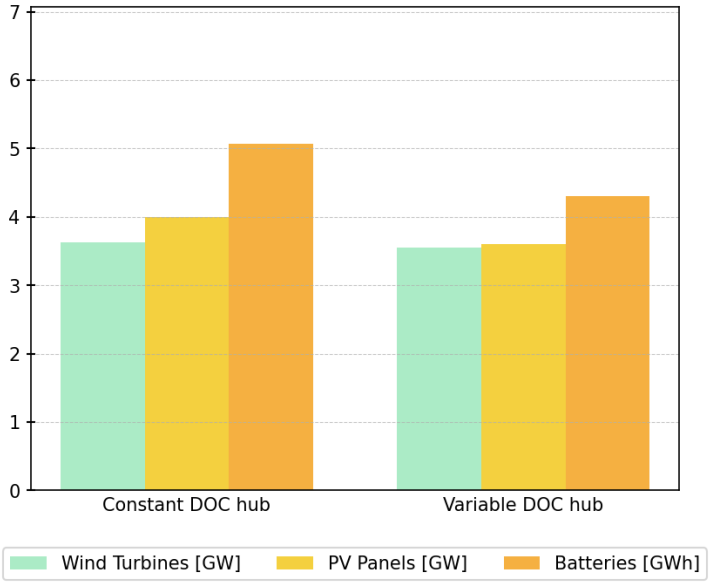

Figure 4.8: Capacities comparison highlighting decrease in installed battery capacity for variable DOC operation.

With the DOC plant no longer required to operate constantly, it can reduce its production during nights and periods of low renewable generation, and consequently its electricity consumption. This adds flexibility that was previously lacking, which was compensated by an increase in production and battery capacity. From the initial 5.03 GWh of installed battery, the scenario with variable DOC now has only 4.30 GWh, thus reducing the total price.

4.3 Summary

The new DOC plant, acting as a replacement for DAC, can prove financially advantageous by lowering the total system prices by 2.94%. Its major advantage is having electricity as its only input, putting aside water and hydrogen inputs that were necessary for air capture.

Despite requiring a higher net quantity of electricity, the introduction of the node results in decreased total installed capacities in PV and wind turbines. Unfortunately, this is offset by the growing need for batteries due to the node's lack of flexibility. This latter point is thus an area for improvement in the technology, given the reduction in total system cost by 6.23% when constant operation is modeled.

New price reductions of 8.30% logically occur when the technology has better techno-economic parameters. Conversely, more pessimistic values for these parameters result in the results being more in line with the reference DAC scenario.

Special attention can therefore be given to this technology showing a real opportunity for the future, as well as the results obtained through the analysis of its implementation, which are summarized for the different simulated scenarios in Tab. 4.4.

Reference DAC Hub	149.7 €/MWh
Reference DOC Hub	145.3 €/MWh
Optimistic DOC Hub	**137.3 €/MWh**
Conservative DOC Hub	156.7 €/MWh
Variable DOC Operation Hub	140.4 €/MWh

Table 4.4: Summary of different prices for each scenario.

Chapter 5

Assessment of Water Usage

In addition to energy challenges, many African countries face a scarcity of water resources, especially in arid region [36]. Finding sustainable solutions for clean water sources aligns with the vision of an RREH, which aims to develop local opportunities. This chapter explores water usage, specifically considering the potential for the designated hub to produce clean water. The goal is to assess the feasibility of providing the hub's surrounding regions with a competitive and sustainable water supply.

For the remainder of this chapter, the DOC will be used consistently in place of the Direct Air Capture, as well as all the new nodes introduced in the previous section.

5.1 Study of clean water

The previous results have demonstrated that water usage was not optimal. Increasing water production by creating a fictional external demand could allow the system to use this commodity as an opportunity to meet local needs without having to make significant changes to the hub operation. Using the hub to produce clean water for local regions also aligns with the Sustainable Development Goals (SDG) of the United Nations (UN), providing additional endorsement for an RREH that complements the goals it already validates (SDGs 6, 7, 8, 9, 12 and 13).

Figure 5.1: EU Sustainable Development Goals [37].

The UN and the World Health Organization (WHO) have declared that a minimum of 20 liters of freshwater per day per person is required to meet basic hydration and personal hygiene needs, 50 liters for a decent standard of living, and starting from 100 liters for real comfort. While developed countries are well above these thresholds, the rest of the world still struggles to access the necessary resources [38] [39].

The population of Algeria being 45.9 million in December 2023 [40], this corresponds to a minimum water consumption of 4590 millions of liters per day only for a personal use.

UNESCO states that domestic uses account only for 22% of liquid freshwater global consumption [41] while the agricultural sector account for 69%. While the report also states that large proportions of the resources consumed come from groundwater or surface water, desalination of water accounts for only a small percentage and is tending to develop further, being an interesting source for arid and coastal regions.

5.1.1 Seawater desalination

The desalination plant have been continuously developed in recent years. While in 2010, the sum of all installations offered an average daily production capacity of 4.6 million m^3, in 2020, this value has increased to 115 million m^3/day when considering the 20 971 existing projects [42].

Joyner E. et al. [42] also presents the various existing technologies and their degree of use. The most widely used technology is reverse osmosis (RO), operating on membranes powered by electricity, accounting for 69% of the installed units. Other installations operate with membranes, but RO has the best energy efficiency.

With a 24% share of installations, the thermal technologies multi-effect distillation (MED) and multi-stage flash (MSF) have interesting efficiencies and properties, but the modeled RREH does not easily produce heat so this technologies will not be considered.

Finally, the remaining existing technologies such as membrane distillation (MD) or forward osmosis (FO) are only used on a small scale, either still in development or not efficient enough.

However, even though the technology is one of the most efficient currently with a conversion factor (See Eq. 3.3) of 2-6 kWh_{el}/t_{H_20} [43] for the desalination of seawater, technology is still in development. While the conversion factor is modeled at 4 kWh_{el}/t_{H_20} in the DOC RREH, research shows that it is possible to achieve values around 1.5 kWh_{el}/t_{H_20} [44] [45]. It will be interesting to see the impact of a change in technical parameters on this unit.

5.1.2 External water demand profile

The earlier discussions in Sec. 4 led to the conclusion that the water desalination unit was underused. This observation hints at the potential of water as a valuable resource within the RREH framework, capable of providing local regions with resources derived from the hub's infrastructure. The integration of an external water demand model becomes essential to understand the system's response to this inclusion and to elucidate the tangible prospects of this conceptual proposal.

Official data on water consumption in Algeria is not freely available, but it is possible to analyze existing studies to recreate similarities in the shape of the demand profile. The study "Predictive Uncertainty Estimation in Water Demand Forecasting Using the Model Conditional Processor" [46] influenced the formation of the modeling. Based on the conclusions of the article, the trends of their curve helped create a realistic representation of a general water demand.

The article already mentioned in Sec. 2.2.3 uses consumption data for a residential area in Egypt (New Borg El-Arab city, Alexandria), serving as a valuable reference for understanding water usage patterns in comparable arid regions. The study illustrates the orders of magnitude in consumption, but also introduces the difference in seasonal demand. The ratio of consumption between seasons is highly variable depending on the meteorological conditions in summer and winter, but it can be considered constant between Algeria and Egypt due to their similar conditions.

By adding the general points such as the shape of the curve profile with the orders of magnitude and the seasonal difference, the external demand for water is modeled with the consumption profile below:

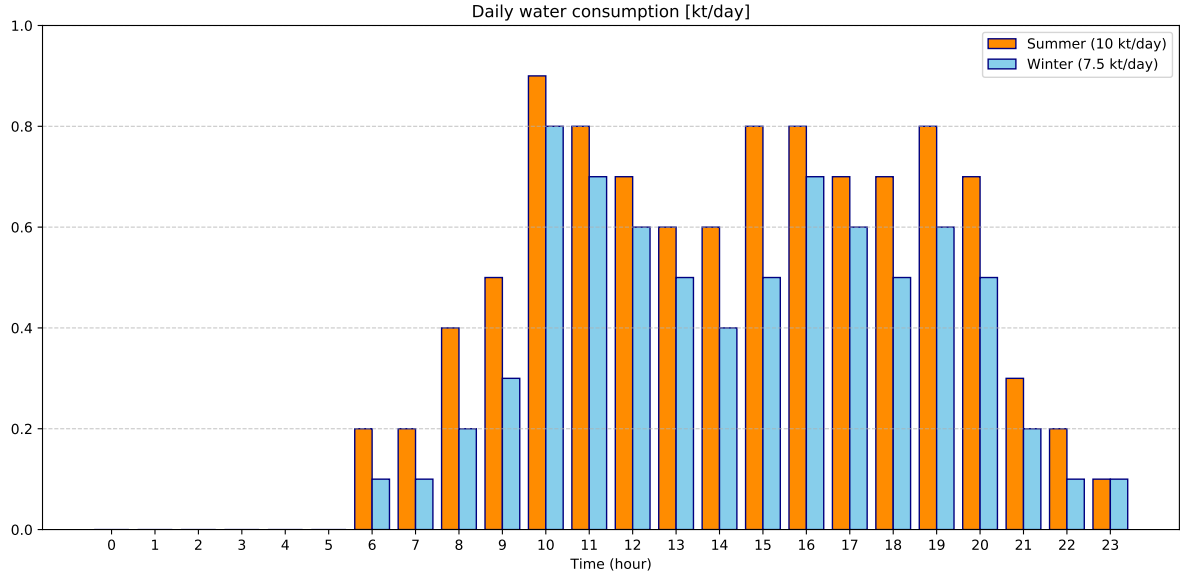

Figure 5.2: Water Demand Profiles with two curves representing summer demand with 10 kt/day and winter demand with 7.5 kt/day. Each hour represent a timestep.

The value of λ_t^e (see Eq. 3.19) therefore takes different values for the 24 time-steps t corresponding to a whole day. The hyperedge e where external demand is set corresponds to the coaster water balance (see App. A.3).

The winter period is considered to be between 20 October and 21 March, and the summer period is the rest of the time, with total quantities of 7.5 kt/day and 10 kt/day respectively. This corresponds to 7 500 000 L/day and 10 000 000 L/day (note: 1 tonne of water is estimated at $1m^3$ and 1000 liters), allowing to supply entire residential area.

5.2 Water Resource Costs

Studying the cost of the system through the various units involved in production is essential to ensure the competitiveness of the system. Previously, the total costs of the system were obtained; however, it is crucial to distinguish the cost associated with methane production and the cost of the external water demand. In parallel with this analysis, the overall behavior of the water system can be understood.

The water price is influenced by various costs such as in Eq. 3.18, where CAPEX and OPEX costs are taking into account. Fig. 4.3 allows us to understand which nodes will contribute to the total cost of water. Firstly, there are the units acting for its production but also the plants that supply these production units. Finally, below is the list of considered plants that are required for external water demand:

- PV Panels
- Wind Turbines
- Batteries
- HVDC
- Desalination Plant
- Water Storage Unit
- Methanation Plant

Some of these nodes are linked to units beyond those engaged in water production, complicating the allocation of costs to either water supply or the methanation process. Hence, to address this, costs will be distinctly attributed to each process using the introduced variables below:

- The **Water Utilization Ratio** ($a_{w,t}$) represents the proportion of water resources used to meet external demand, providing insights into the allocation of water within the system. It is calculated based on the fraction of water directed to external demand relative to the total water output.
- The **Electricity Utilization Ratio** ($b_{e,t}$) signifies the portion of total electricity consumed by the system allocated to fulfill the external water demand
- The **Installed Capacity Growth Ratio** (c^n) indicates the increase in installed capacities dedicated to meeting external water demand. It is expressed as the proportion of installed capacity specifically allocated to water demand relative to the total installed capacity for each participating node.

The water price is then determined by adding these costs and dividing by the total quantity of water produced by the system over the same period. This method allows for assigning a unit cost to each cubic meter of water produced.
It is important to note that the calculated costs only include those related to water treatment; the distribution of water also has a significant cost.

5.2.1 Water utilization

The variable $a_{w,t}$ denotes the proportion of the total water produced in the system that is allocated to meet the external water demand. It is expressed as:

$$a_{w,t} = \frac{\lambda_t^w}{\sum_{n \in \mathcal{N}^w} \; q_{w,t}^n} \tag{5.1}$$

λ_t^w : External water demand at timestep t
$q_{w,t}^n$: Outgoing quantity of water w from node n at timestep t
$\mathcal{N}^w$: Set of water-producing nodes (desalination plant, storage unit, methanation plant)

This variable provides insight into the allocation of water resources in the system. The first 800 values are illustrated in Fig. 5.3 for better visibility, but the overall behavior remains the same throughout the time horizon. The rapid variations correspond to those related to the profile of the external demand. Logically, when the demand is zero, all water is used for methane production, and the variable is 0.

The variable takes highly fluctuating values ranging from 0 (when the demand is zero) to almost 1 (when the demand is maximal), once again demonstrating that the amount of water required for methane production is minimal (used only by the electrolysis plant). The values will undoubtedly affect the water costs associated with the units producing in a significant manner.

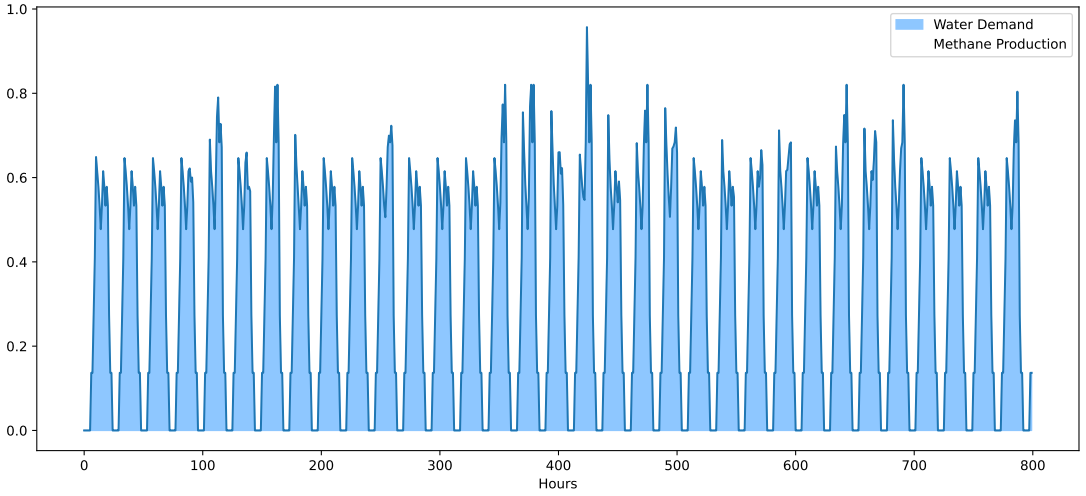

Figure 5.3: Representation of the variable $a_{w,t}$ according to time in hours, i.e. percentage of water resources used in the entire system to meet external demand.

5.2.2 Electricity utilization

The variable $b_{w,t}$ denotes the proportion of the total electricity used by the system that is allocated to meet the external water demand. It is expressed as:

$$b_{w,t} = \frac{(\sum_{n \in \mathcal{N}^w} \; q^n_{e,t})\; a_t}{q^H_{e,t}} \tag{5.2}$$

$q^s_{e,t}$: Electricity e used by node n at timestep t
$\mathcal{N}^w$: Set of water-producing nodes (desalination plant, storage unit, methanation plant)
$q^H_{e,t}$: HVDC incoming power e at timestep t

This variable provides insight into the utilization of electricity in the system. Fig. 5.4 shows the first 800 values of the variable b_t, highlighting the daily variations associated with the demand profile. It is interesting to note that the major peaks in usage correspond to moments when significant peaks in water resource usage are present, and the values do not exceed 0.007, affirming that the external demand does not allocate a large amount of electricity, which will not significantly affect the price of water.

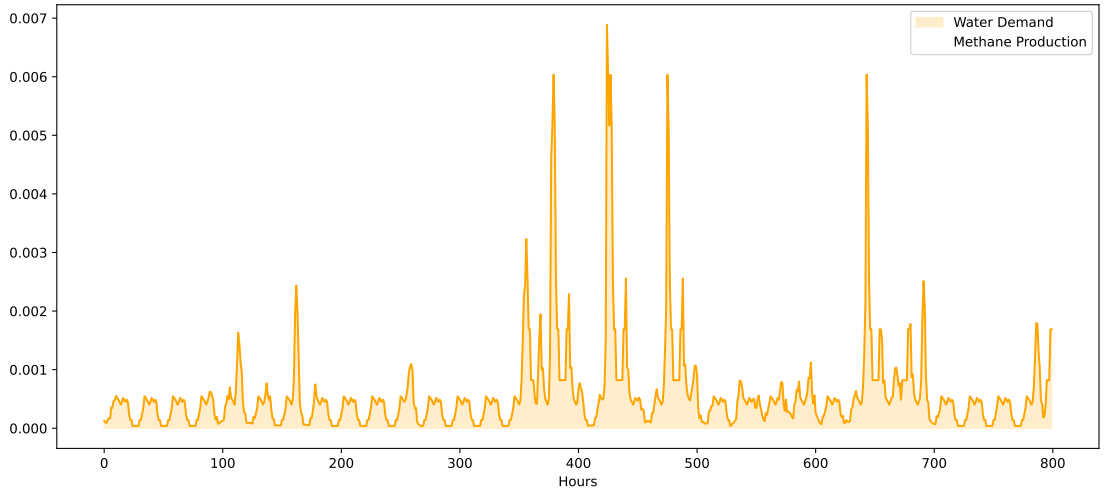

Figure 5.4: Representation of the variable $b_{w,t}$ according to time in hours, i.e. percentage of electricity used in the entire system to meet external demand.

5.2.3 Installed capacity growth

The variable c^n denotes the proportion at node n of the installed capacity invested to meet the external water demand. This proportion is defined as the installed capacity specifically allocated to the water demand relative to the total installed capacity, for each node participating in meeting the demand. It is expressed as follows:

$$c^n = \frac{K^n - \bar{K^n}}{K^n} \tag{5.3}$$

K^n : Installed capacity of node n with water demand
$\bar{K^n}$: Installed capacity of node n for without water demand

This variable provides insight on the increase in installed capacities due to the integration of an external water demand. This analysis is performed on all units involved in meeting the water demand, including everything related to electricity, PV Panels, wind turbines, batteries, HVDC, and also concerning water, the desalination plant and the storage unit.

5.2.4 Water Price

Using the three variables defined above, it is therefore possible to calculate the Total Water Costs (TWC) as follows:

$$\text{TWC} = \sum_{n \in \mathcal{N}^a} (\sum_{t \in \mathcal{T}} q^n_{w,t}\, a_{w,t}\, \theta^n) + \sum_{n \in \mathcal{N}^b} (\sum_{t \in \mathcal{T}} q^n_{e,t}\, b_{w,t}\, \theta^n) + \sum_{n \in \mathcal{N}^c} \mathcal{C}^n\, c^n \tag{5.4}$$

$\mathcal{N}^a$: Set of water-related nodes (H_2O Storage, methanation and desalination plant)
$\mathcal{N}^b$: Set of electricity-related nodes (PV panels, wind turbines, batteries and HVDC)
$\mathcal{N}^c$: All nodes linked to external water demand ($\mathcal{N}^a \cup \mathcal{N}^b$)
$q^n_{w,t}$: Outgoing quantity of water from node n at timestep t (kt/h)
$q^n_{e,t}$: Outgoing quantity of electricity from node n at timestep t (GW)
θ^n : VOM of node n
$\mathcal{C}^n$: Costs related to CAPEX and FOM of node n

The following relationship allows obtaining the price of water per m^3, enabling comparison with general data. This is expressed as:

$$Price_w = \frac{TWC}{(D_w\, n_w + D_s\, n_s)\, T} \tag{5.5}$$

D_w : Total demand for one day in winter (e.g., 7.5 kt/day)
D_s : Total demand for one day in summer (e.g., 10 kt/day)
n_w : Number of days when winter demand is applied
n_s : Number of days when summer demand is applied
T : Time horizon

The cost breakdown of the water demand provides a detailed visualization of the major components contributing to the total costs. Each colored segment of the horizontal bar in Fig. 5.5 represents a specific category detailing how the expenses are distributed. The value at the center of each section indicates the cost associated with that category, while the total value at the end of the bar represents the overall cost of water demand amounting to 3.09 €/t.

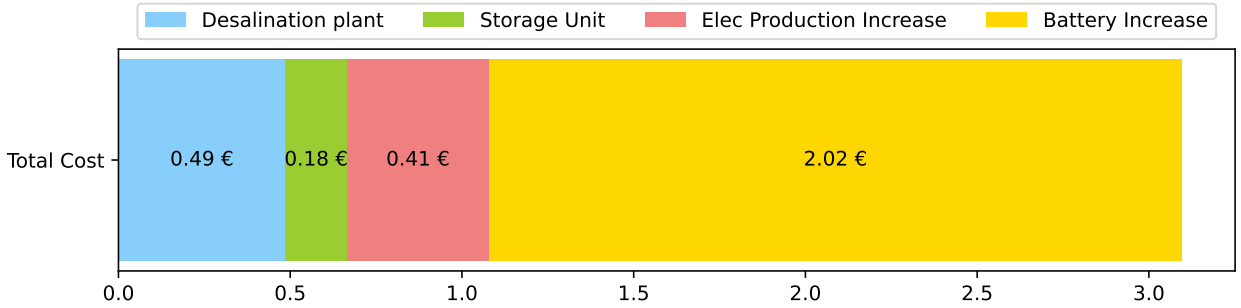

Figure 5.5: Water Costs Breakdown for reference scenario (Total: 3.09 €/t).

The costs related to the increase in water storage are represented at a low proportion because operating costs are neglected in the modeling. The minor expenditure is thus related to the installation of new capacities, a conventional and affordable construction, which is necessary due to the variability in demand within a single day.

Then come the category of the desalination plant which logically must process a larger quantity of water, increasing the installed capacity and its operating costs. With the same proportion, the increase in electricity generation comes from the fact that the use of technologies for desalinating water (operating with electricity) is amplified. In particular, the desalination plant has a constant consumption due to its continuous operation, and the storage unit consumes when water is brought in.

Finally, the largest proportion is related to the increase in installed battery capacity as well as its operating costs. This observation is due to the constant consumption of the desalination plant even during the night when most RE sources are down. Additionally, during the night, the water storage unit is in operation to store the surplus water which will be released during the day when the external demand is higher (See Fig. 5.6).

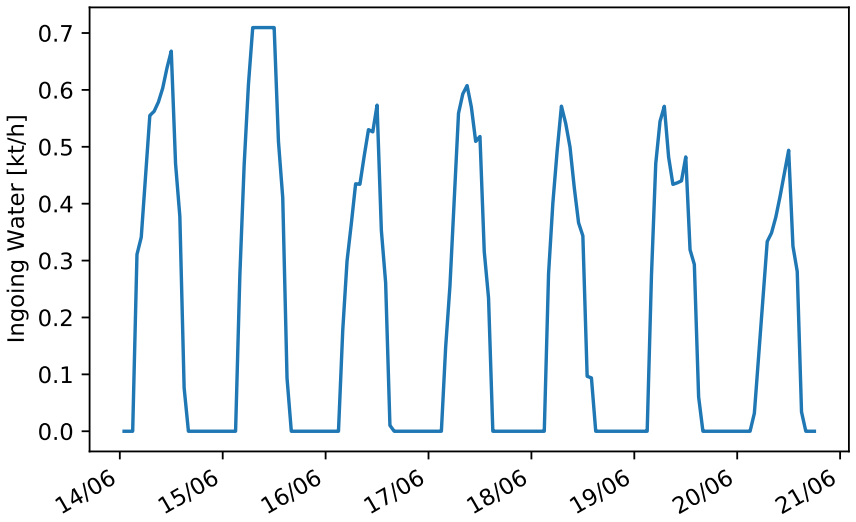

Figure 5.6: Water entering the storage unit (kt/h) for couples of days showing pics during nights when the storage unit fills itself to pour out the day.

Fig. 5.7 compared the dual values obtained for each hour (see Sec. 3.2) and the values of water demand over a year. The graph is too small to observe the variations in demand over the course of the days, but it does help in easily seeing the maximum demand based on the period throughout the year. Through this graph, several conclusions can be drawn:

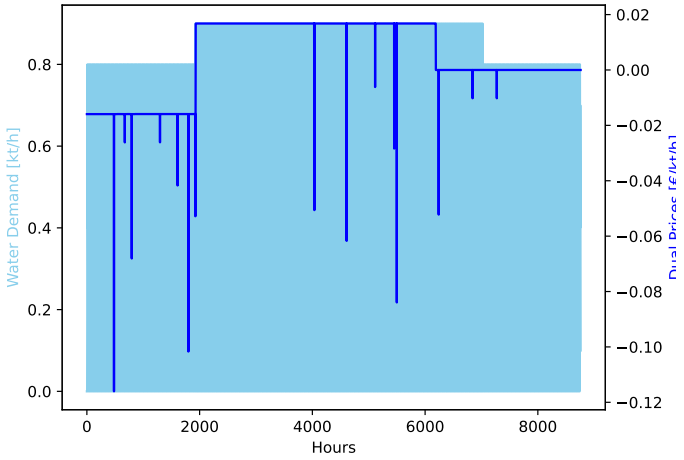

Figure 5.7: Dual prices along with water demand. Negatives values appears at the same time as winter demand means that the system is undersized at this time. Reverse thinking is done for positive values. Fallen picks appaers when storage unit release extra-water.

Positive values appear when the demand is higher, indicating that the resource is limited. Indeed, to increase water production by one unit, it would be necessary to either increase the installed capacity of the desalination plant or the storage, resulting in a higher relative cost.

Negative values indicate that the resources allocated to water production are underutilized, and producing an additional unit of water would result in a decrease in the associated relative cost. The facilities needed for higher demand in the summer are also available during the winter, over-sizing the system during that period.

Falling picks appear about a dozen times throughout a year. The dual value drops suddenly because the resource is underutilized during this period. This corresponds to the time when water is overproduced while the demand is met simultaneously, so that the storage system is completely filled, and water must then be released into the environment (due to the relaxation of the constraint). Fig. 5.6 illustrates this phenomenon that occurs on 15/06 when the storage unit is filled for several consecutive timestep.

Recovering the dual prices allows for capturing this phenomenon that occurs only rarely throughout the year which, with dual prices, can demonstrate the optimality (or not) of the system.

Tab. 5.2 allows for a comparison of the price obtained for the hub with those of competitive systems in some European countries. Although more expensive than the majority, the water produced by the hub has a reasonable price that could be realistic. In the following section, different configurations will be considered to see how the price per tonne can evolve in a positive direction.

Italy	0.67 €/t
Spain	1.90 €/t
France	2.1 €/t
Belgium	2.37 €/t
Germany	2.78 €/t
Remote Hub	3.09 €/t
Portugal	3.23 €/t
England	3.77 €/t

Table 5.1: Water treatment prices in Europe [47] compared to the water remote hub.

5.3 Analysis of adjustments: Impact on Water Prices

This section focuses on examining modifications in the system, including changes in external water demand and amelioration of the techno-economic parameters of the desalination plant. The aim is to assess how these modifications influence the behavior of the system and, consequently, impact the water price.

5.3.1 Improvements of desalination technology

As discussed in Sec. 5.1.1, the conversion parameter of the desalination plant can be changed in a more optimistic way, such that $\phi_1 = 0.002\ GWh_{el}/kt_{H20}$, which doubles the efficiency of the node (see Tab. A.1).
Fig. 5.8 displays the results with a water price of 2.92 €/t.

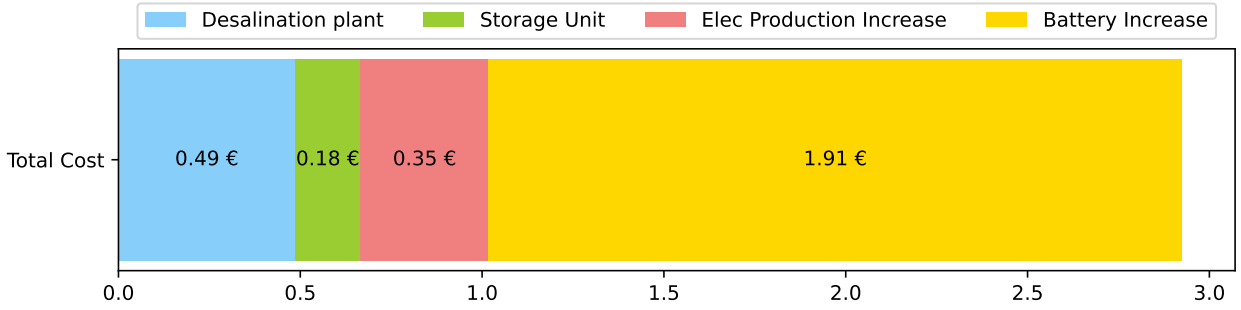

Figure 5.8: Water Costs Breakdown for improvement in desalination (Total: 2.92 €/t).

The improved efficiency of the desalination node results in a reduced electricity consumption while producing the same amount of water.
Therefore, the price of water decreases due to the reduced need for an expansion in electricity production capacity. However, the installed capacity required for batteries remains significant which results in the price.

5.3.2 Constant summer demand

The analyses related to Fig. 5.7 led to the conclusion that the system was oversized during winter demand periods, resulting in lost of earnings reflected in the water price. To address this, the summer demand will be applied consistently throughout the entire time horizon.
Fig. 5.9 displays the results with a water price of 2.81 €/t.

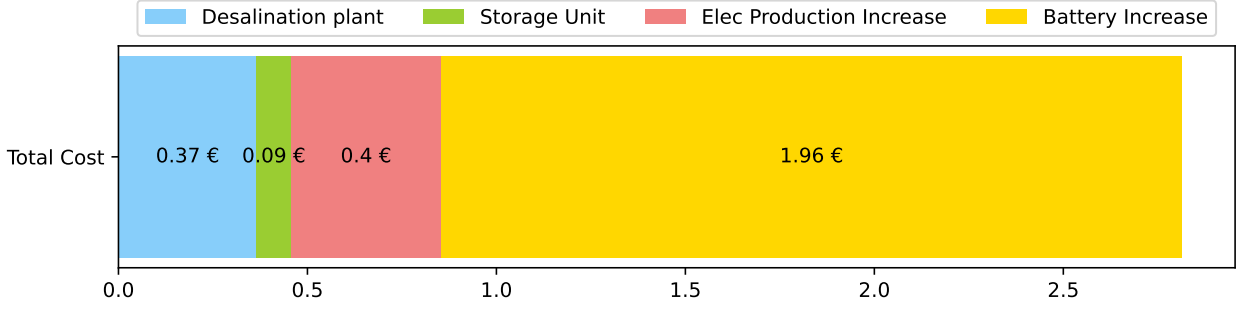

Figure 5.9: Water Costs Breakdown for constant summer demand scenario (Total: 2.81 €/t).

The reduction in price is attributed to the utilization of existing infrastructure employed for seasonal demand, where a greater volume of water is produced. Setting $n_s = 365$, as described in Eq. 5.5, leads to a decreased cost per ton.

Furthermore, battery storage is reduced with an installation of 4.17 GWh compared to 5.03 GWh previously required because the filling of water storage units is less significant; the previous overproduction is now dedicated to external demand. Therefore, it is optimal to use the facilities to the maximum and produce as much as possible relative to the installed capacities.

5.3.3 Variable desalination operation

The desalination plant is modeled to operate constantly ($\mu^n = 1$ in Eq. 3.7); however, this has proven to be a drawback in the system behavior as it often overproduces. To assess the impact of a variable operating mode, the parameter will be set to $\mu^n = 0.7$
Fig. 5.10 displays the results with a water price of 2.88 €/t.

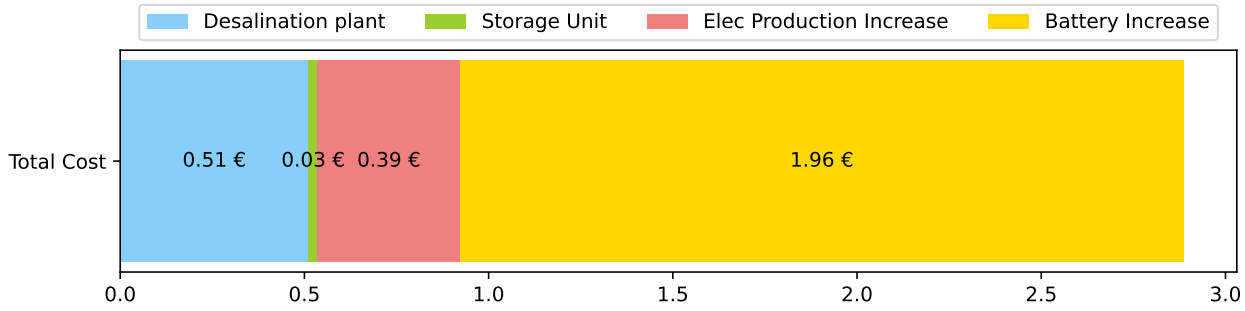

Figure 5.10: Water Costs Breakdown for variable desalination operation (Total: 2.88 €/t).

Fig. 5.11 explains the drop in water price by highlighting that the resources allocated to water production are well adapted to the external demand for water, since the dual values are mainly zero and falling picks are rare. The desalination plant is now used judiciously, as its water output follows the profile curve of the external water demand. This leads to an increase in the use of the desalination plant and a reduction in the need for water storage.

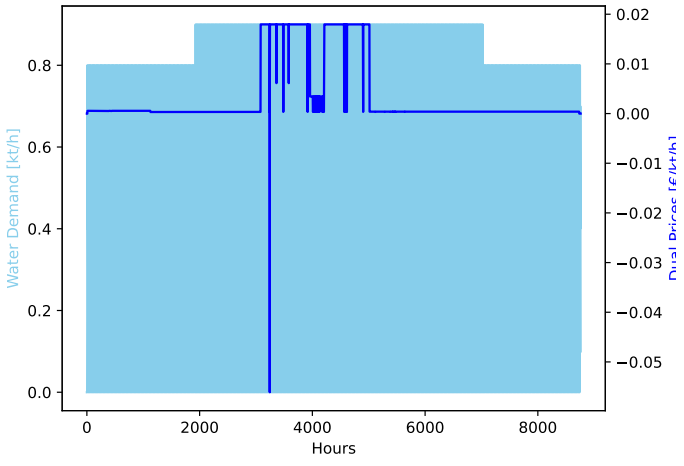

Figure 5.11: Dual prices in parallel with water demand.

Moreover, there is a reduction in renewable production installations and batteries as the energy demand decrease during the night, moment where water facilities functioned unnecessarily resulting in an excess of water.

5.3.4 Combining previous improvements

Finally, it is interesting to see the impact of the three previous changes applied all at once, i.e., $\phi_1 = 0.002\ GWh_{el}/kt_{H_2O}$, $n_s = 356$ and $\mu^n = 0.7$.
Fig. 5.12 displays the results with a water price of 2.63 €/t.

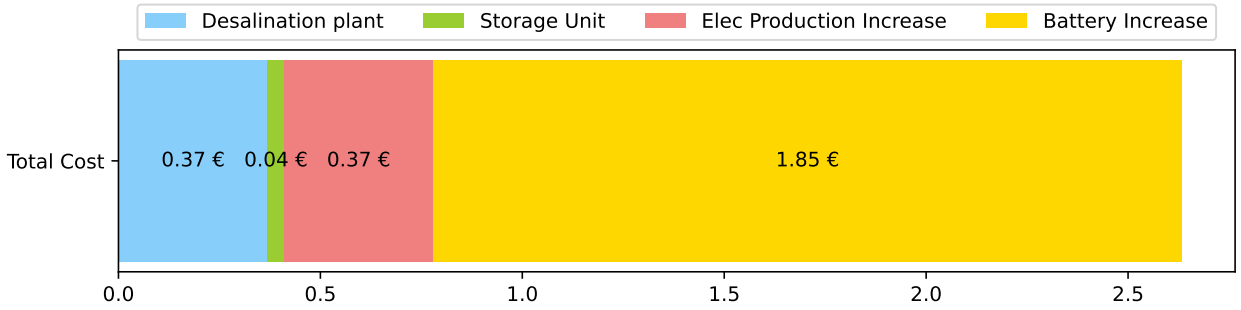

Figure 5.12: Water Costs Breakdown when combining all previous improvements (Total: 2.63 €/t).

This configuration further lowers the price, while incorporating all the advantages mentioned earlier. The electricity consumption is reduced by improving the efficiency of the desalination plant, which operates in coordination with external water demand and is used optimally by producing as much as possible, reducing the need for water storage units.

5.4 Summary

The analyses have demonstrated the possibility for an RREH to meet external water demand while maintaining competitiveness. Potential improvements or changes in configurations also allow for total price improvements, particularly by ensuring desalination plant operation aligned with optimal external demand. All results are summarized in Tab. 5.2.

Classic water demand configuration	3.09 €/t
Improvement of desalination technology	2.92 €/t
Constant summer demand	**2.81 €/t**
Variable desalination operation	2.88 €/t
Combining all improvements	**2.63 €/t**

Table 5.2: Water prices depending on water demand configurations.

Chapter 6

Multi-hub Configuration

This chapter introduces new locations where RREHs are implemented, on the one hand to compare their own efficiency and on the other hand to introduce the idea of multi-hub, where their simultaneous implementation would make it possible to see potential connections between them and determine whether interactions are taking place.

6.1 Context and objectives

While most studies of energy hub implementation are limited to considering one RREH used to power one load center, this work will examine the implementation of multiple RREHs that can power multiple load centers. This is in accordance with the idea developed in Sec. 2.3 of the global grid concept.

In the same way as renewable energies can supply a power grid according to their output at a given time, alleviating the problem of intermittence, the various RREHs operating in the four corners of the world could supply the load centers of their Power-to-X products depending on their availability. This joint collaboration between hubs is designed to reduce the total cost of products supplied to load centers through their interaction.

At first it is necessary to locate areas where hubs could be installed, where the location meets the necessary conditions (no nearby urban area, adjacent to a significant water source for desalination, near an area where boats can start,..). The criterion that will determine the final locations chosen will be the renewable power density related to climate conditions, namely the photovoltaic potential and the wind energy density. The presentation by Dachet V. et al. (1)(2023) [3] exposes sites with high renewable potential as well as areas with high population density, showing the mismatch between the two and how the multi-hub concept could solve this.

One concept that has not yet been sufficiently developed is the modeling of shipping. Berger M. et al. [5] (2021) implements the journey between its RREH in Algeria and its load center in Belgium so that the distance is always fixed. Dachet et al. (2)(2023) [21] took on the same working bases by implementing an additional RREH in Greenland, but as the distances between Greenland-Belgium and Algeria-Belgium were approximately the same by ship, there was no need to consider a change in modeling.

6.2 Implementation and data recovering

As mentioned previously, the remote areas chosen for an RREH installation must have either very high photovoltaic potential, or very high wind power density, or a mixture of both. This will have an impact on the quality of capacity factors, which are essential to consider when creating a hub, as explained in Sec. A.3. Renewable potential maps can be used to guide the search for interesting areas, and to confirm the potential, the *RenewableNinja* website provides capacity factors for any location in the world to be retrieved.

Load centers will be chosen so as to provide easy access to energy markets, i.e. in high-density population areas. All the selected areas meeting the expected criteria are shown on the world map in Fig. 6.1.

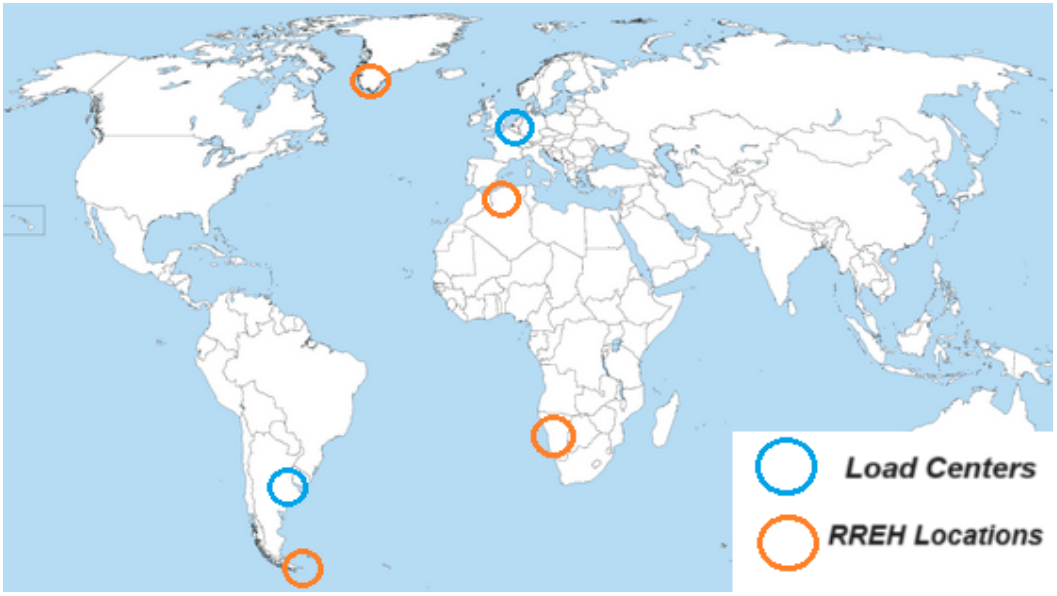

Figure 6.1: World map showing four selected RREH locations providing methane to load centers.

The Algerian region is included here, so that other locations can be compared with an already known location. As a reminder, solar panels and wind turbines are placed in a desert, a region combining high irradiation and abounding winds.

Greenland has also been taken into account, as work already carried out by Radu D. et al. (2019) [23] has shown that its particular wind conditions offer great renewable potential.

Then the next location considered is rather exotic, in Namibia. The vast plains along the coast have similar meteorological characteristics to Algeria, which can be compared by simulation. Developing an RREH in Africa would also have an interesting social side, by creating industries, jobs or valorizing by-products.

The last region considered for a RREH is located at the southernmost point of South America, Cape Horn on the Chilean side. This great cape is known for being one of the hardest places for trading ships to cross, due to strong storms and violent waves. The winds passing through the area are therefore strong and abundant, giving an interesting renewable potential despite the lack of irradiation due to the high latitude.

Figure 6.2: Map focusing Cap Horn, South American southernmost location.

These four locations were chosen for their advantageous weather conditions. Tab. 6.1 quantifies this by comparing mean solar and wind capacity factors of each locations, derived from data taken for each hour over a period of one year, which will be used for PV panels and wind turbines modelling. To make the data representative, three points from each location were take for their capacity factor in order to average them. At first look, Algeria and Namibia have similar conditions, while Greenland, considered for its advantageous winds, is being swept away by those of Cap Horn.

The first load center considered is located at the same position in Europe as previously. It will serve as a reference for economic comparisons between each hub taken individually. The second load center is on another continent, near a densely populated region. Although Brazil would have been a good choice, the one made here is Argentina, near Buenos Aires.

Each location considered for the installation of an RREH will have the same design as shown in Fig. 6.3, with the exception of Greenland and Cape Horn which will have no PV panels. Each load center will also have the same layout for its own destination.

	Algeria	Cap Horn	Namibia	Greenland
Mean Wind Factors	50%	72.3%	52.1%	56.2%
Mean Solar Factors	24.6%	/	23.5%	/

Table 6.1: Mean capacity factors of selected locations to install RREHs.

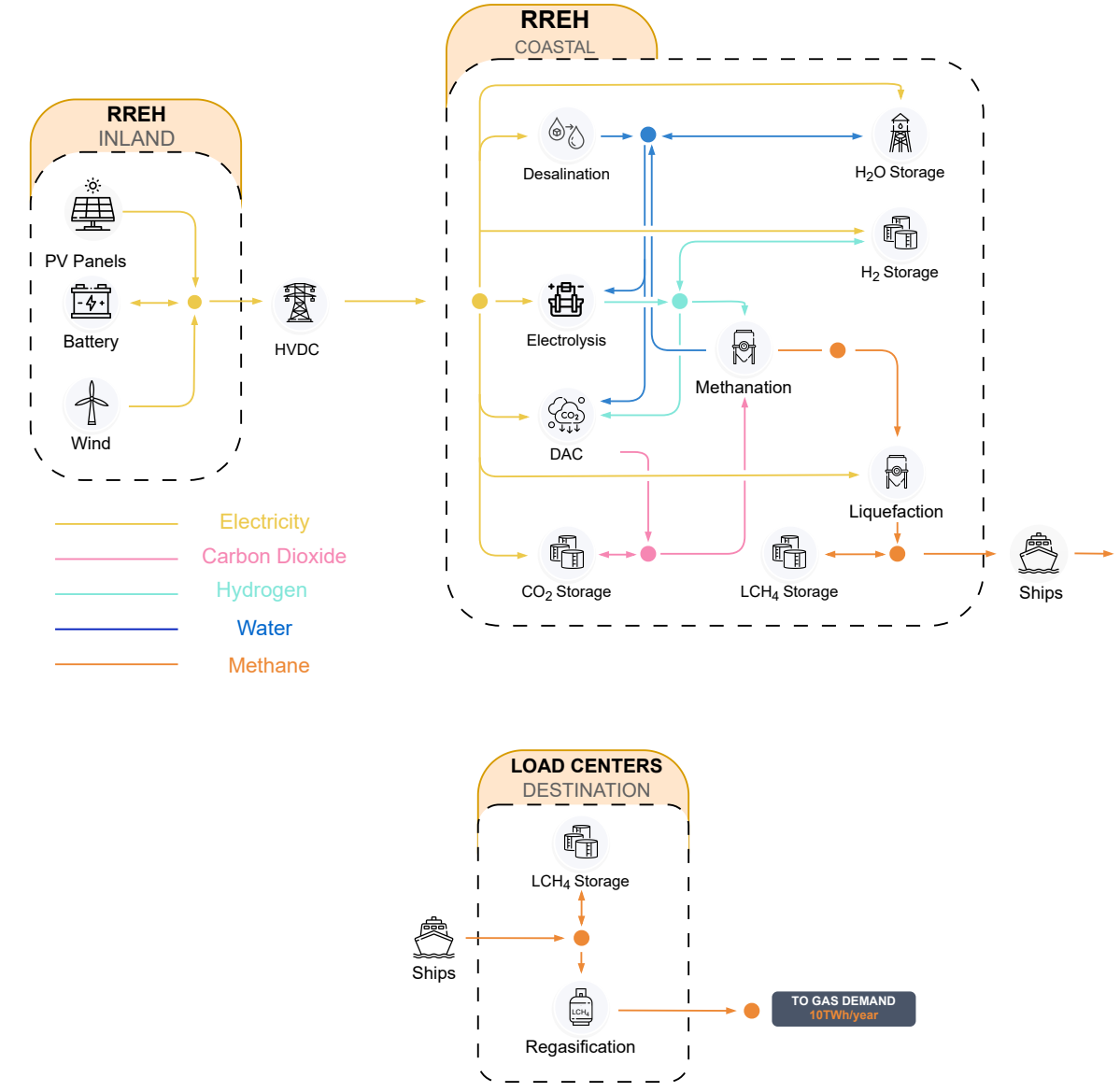

Figure 6.3: Illustration of the major module used to model all four RREHs along with the one used to model load centers.

6.2.1 Travel costs

A very important parameter in ship modelling is the conversion factor of its associated node, equivalent to the losses the boat assumes by consuming part of the fuel it carries, to move forward. This is a decisive factor in the sizing of the RREH, since higher transport losses would lead to an increase in the installed capacity of all the preceding units in the supply chain.

Berger et al. (2021) [5] takes into account the value of 0.125% per day of losses, equivalent to a loss factor of 0.000052 -/h. However, they apply it directly to their journey time, while this ratio will have various journey itineraries. The formula that takes loss factor and travel time into account is expressed as:

$$\text{Conversion Factor} = (1 - \text{Loss Factor})^{\text{Travel Time}} \tag{6.1}$$

However, placing the new variable as an exponential could create numerical problems. The following formula is therefore proposed:

$$\text{Conversion Factor} = 1 - \text{Loss Factor} \times \text{Travel Time} \tag{6.2}$$

This proposal is perfectly acceptable, given the small difference in conversion factor, as shown in Fig. 6.4, even for travel times of several hours.

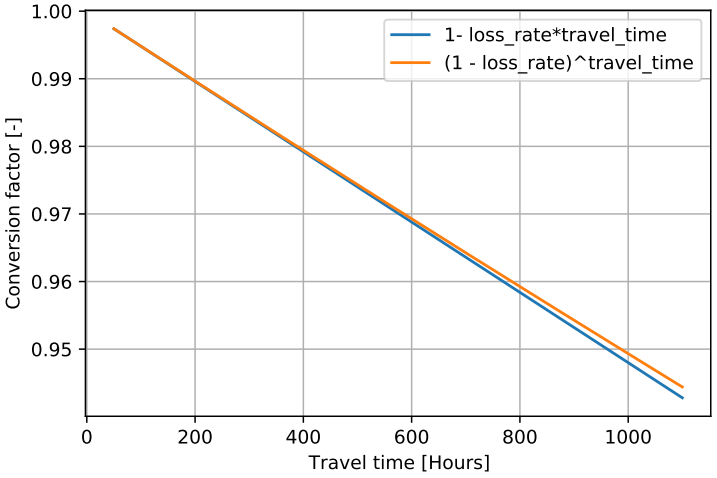

Figure 6.4: Conversion factor according to travel time for exponential and multiplication equations. No difference is made even for several hours of travel.

Each carrier schedule is therefore also adapted to correspond to the journey times and their loading times, which has the basic value of 24 hours. Tab. 6.2 shows all possible ship paths, their travel times and their conversion factors.

Path description	**Travel Time [hours]**	ϕ_1 [/]
Algeria - Europe	116	0.9939
Cap Horn - Europe	400	0.9792
Namibia - Europe	310	0.9839
Greenland - Europe	94	0.9951
Algeria - Argentina	312	0.9838
Cap Horn - Argentina	70	0.9964
Namibia - Argentina	193	0.9899
Greenland - Argentina	343	0.9822

Table 6.2: Full description of each possible ship path.

6.2.2 Results

As a first step, each RREH location will be modeled individually with a single load center in Europe with a demand of 10 TWh per year. Tab. 6.3 shows methane prices before and after regasification. Values for liquid methane are considered just after liquefaction, i.e. in the hub itself. The cost of ships, which varies according to each location, is therefore deducted in this case.

	Algeria	Cap Horn	Namibia	Greenland
Cost to hub in €/MWh [Liquid]	146.0	**126.1**	148.4	199.2
Cost to Europe in €/MWh [Gaseous]	149.7	**129.7**	151.9	202.9

Table 6.3: Methane costs in €/MWh for each RREH location, showing a great potential at Cap Horn with its powerful and abundant winds.

Costs partially reflect the analysis made on capacity factors. Indeed, the better the climatic conditions are, the less installed capacity is needed to produce power. Cap Horn would therefore be the most interesting location, followed by Algeria and Namibia which are similar. The worst is therefore Greenland, which seemed promising in view of the mean wind factors. Tab. 6.4 illustrate installed capacity in PV panels and wind turbines for each RREH locations as well as installed battery capacities.

The installed battery capacity shows that flexibility is therefore the weak point of Greenland, which despite strong winds, are not constant. Fig. 6.5 compares wind factors with those of the Cap Horn for the first hours and shows the difference between wind frequencies.

	Algeria	Cap Horn	Namibia	Greenland
Wind capacity [GW]	4.3	3.88	4.14	4.66
Solar capacity [GW]	4.3	/	4.36	/
Battery capacity [GWh]	2.78	4.22	3.29	16.47

Table 6.4: Installed capacities of PV panels and wind turbines for each RREH location providing fuel to Europe. Algeria and Namibia have similar values while Cap Horn installs much less capacity due to more abundant winds than in Greenland as shown by the installed battery capacities.

There are therefore many times in Greenland where it is not possible to produce electricity, hence the important capacities of storage units regulating flexibility. Fig. 6.6 shows the impact that this has on the cost of the hub in Greenland, the system being oversized.

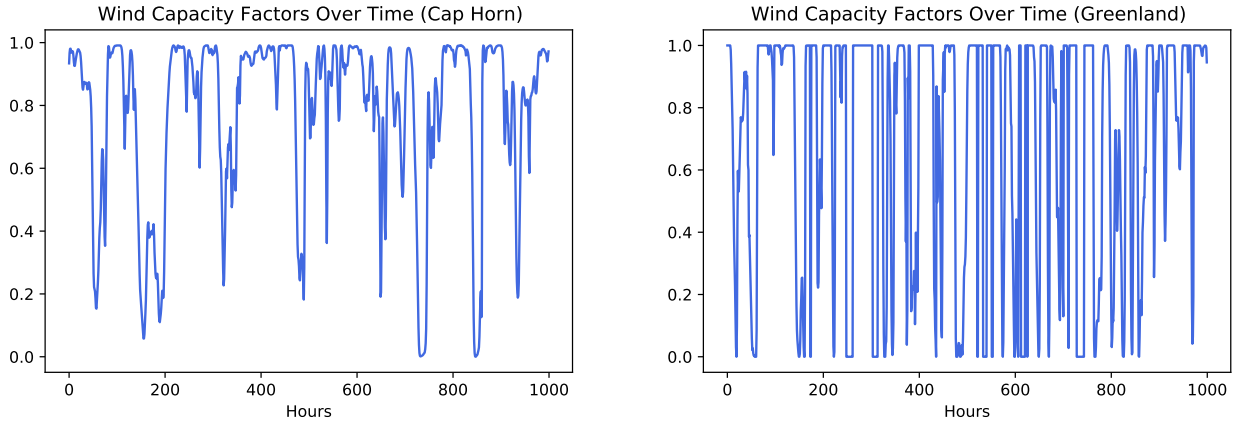

Figure 6.5: Comparison of wind capacity factors of Cap Horn and Greenland, highlighting the best wind frequency for the first location.

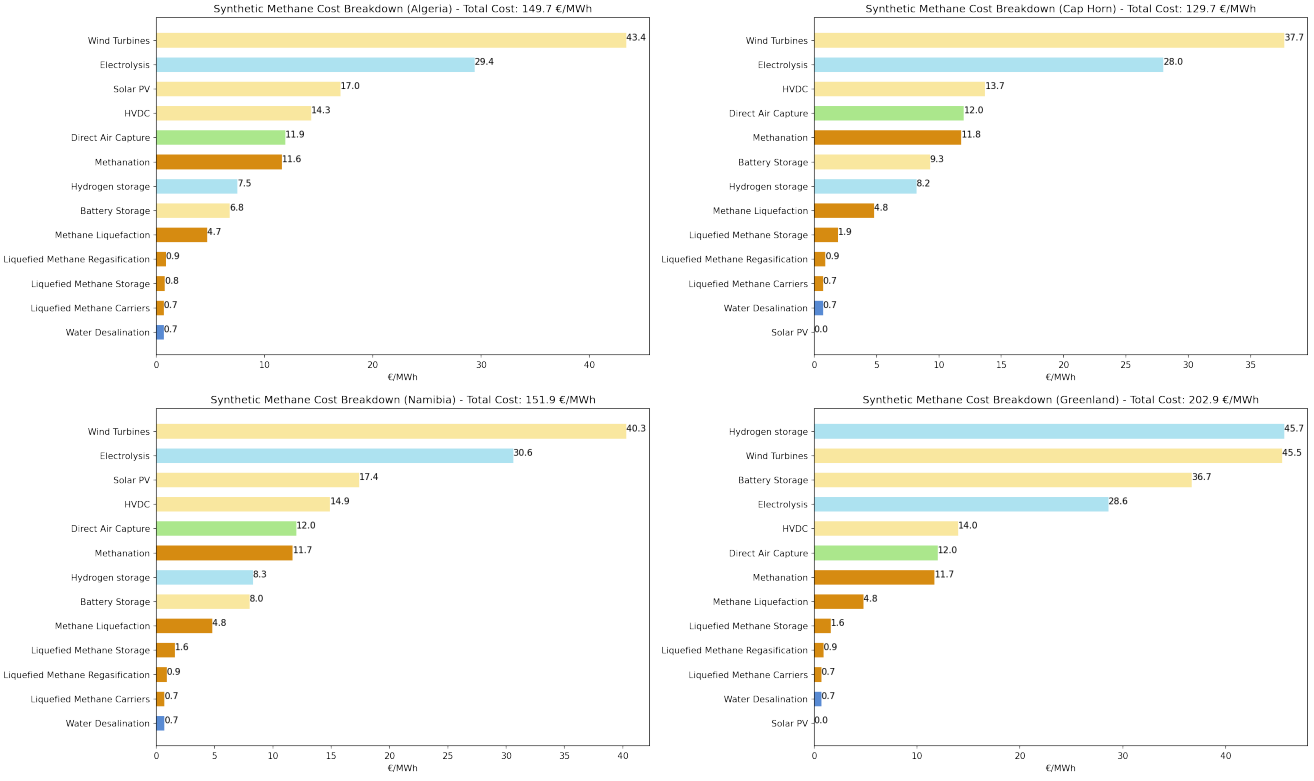

Figure 6.6: Cost breakdown of methane in €/MWh (HHV) for each RREH locations providing European markets. Highlights high costs of Greenland caused by the lack of flexibility and therefore large storage capacities, in contrast to Cap Horn.

6.2.3 Multi-hub limitations

The next logical step in the analysis is to integrate the four hubs into a single simulation providing both load centers. To achieve this, the modeling is done in such a way that any hub can supply any load center. Exchanges between RREHs are therefore not taken into account, although this could have been interesting, particularly for the transfer of captured CO2 between hubs.

The external demands of load centers will be arbitrarily set at 10 TWh/year for Argentina and 20 TWh/year for Europe. No constraints are set on hubs so they can install as many installations as they require.

The result in Fig. 6.7 is disappointing and clearly shows the limits of linear optimization, the model installing only one RREH on the Cap Horn location. Although this would have been predictable, this configuration is not necessarily realistic and desirable given the lack of interconnections between the hubs. The model chooses the most economically advantageous location without taking into account installed capacity values that may be too large for the location in question.

In the end, despite the addition of the impact of the conversion factor changing with travel distances, the loss factor remains negligible for it to have a real impact on the system. In order for the model to begin to really penalize long-distance travel and not install only one RREH in Cape Horn, the loss factor would need to be 8 times greater than it is currently, which would result in a loss of 1% of cargo per day of travel (compared to 0.125% currently).

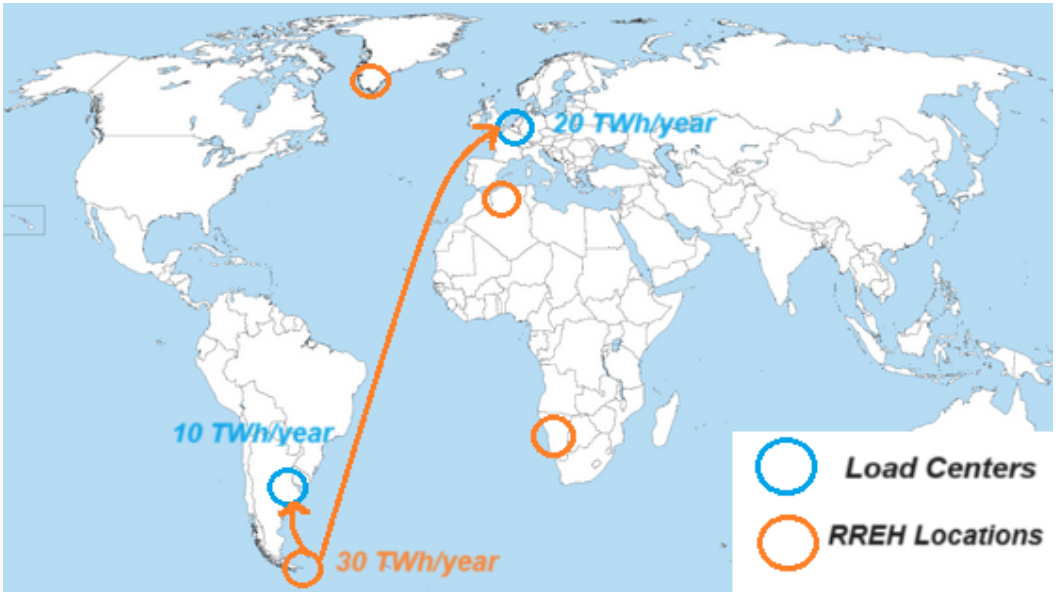

Figure 6.7: World map with load centers with a total methane demand of 30 TWh/y. Cap Horn provides on its own 30 TWh/y as it is more economically advantageous than other locations.

The same conclusions will be drawn as in the previous section, namely to know the best hubs economically. Cap Horn was the most profitable location, so the model meets effectively the previous analysis. Fig. 6.8 shows that when restrictions are applied to this RREH, so that it produces a maximum of 15 TWh/year, the second best rental economically speaking is prioritized by the model, namely Algeria.

Additional constraints could then be added, for example to respect the actual space available on the sites, and the model will install as much as possible in Cape Horn, Algeria, then Namibia and so on until it can provide the overall external demand of each load centers.

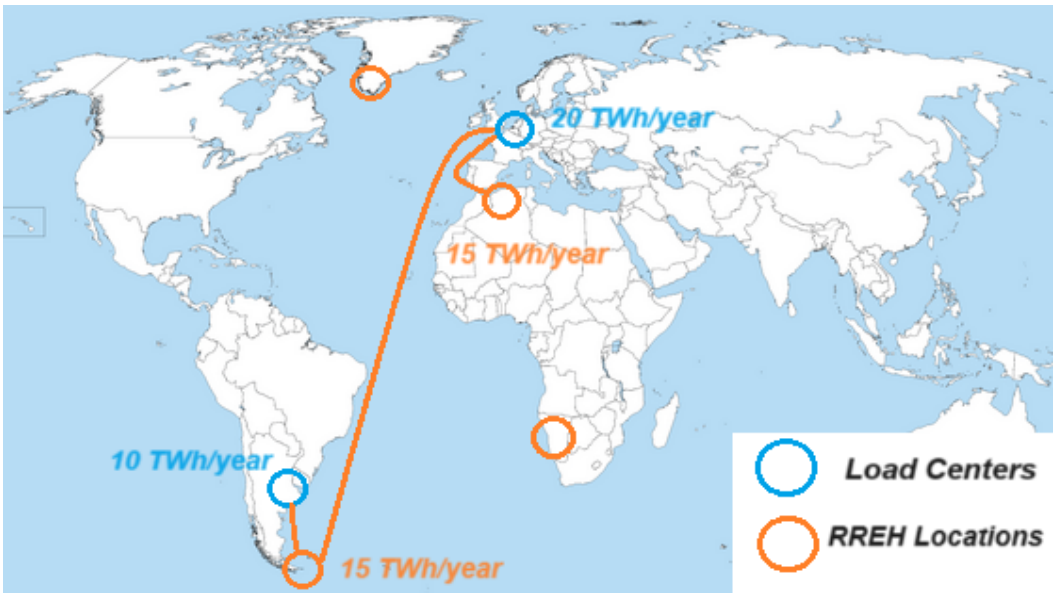

Figure 6.8: World map with load centers with a total methane demand of 30 TWh/y. Cap Horn being forced to provide 15 TWh/y maximum, Algeria provided the rest of the methane being the second best location.

Chapter 7

Synthetic Fuels to decarbonize transport and aviation sectors

This chapter introduces the production of synthetic fuel oil via the Fischer-Tropsch (FT) reaction from pure hydrogen molecule and carbon dioxide. FT-products can then be used for the same purposes as in the conventional oil industry. An economic report will be made as well as a sensitive analysis to capture the reactions of the system to the unexpected variations.

7.1 Context and Objectives

While international agreements, such as the Paris Agreement 2015, aim to significantly reduce greenhouse gas emissions across all sectors by mid-century to limit global warming to 1.5°C by the end of this century [48], some sectors face challenges in decarbonizing. This is particularly the case for transportation-related lines of activities which constitutes nearly a quarter of the total CO2 emissions worldwide, whether it be road or air transport. The IEA graph illustrates the past and expected evolution of CO2 emissions from various types of transportation [49].

The concept of Power-to-X (see Sec. 2.2.2), introduced and previously used for methane, can also be utilized to create synthetic liquid fuels for decarbonizing these sectors. The conversion of H2 and CO2 via Power-to-Liquid (PtL) allows for the production of a carbon-neutral synthetic fuel, because despite its future combustion, it will have been created from CO2 captured from ambient air through Direct Air Capture (DAC) (see Sec. A.1) creating a carbon-neutral loop.

The PtL mechanism can be done in several distinct ways, but the reaction used here will be the Fischer-Tropsch (FT) process. As indicated in Umwelt Bundesamt [50], PtL pathway through Fischer-Tropsch offers a high degree of technological readiness due to the widespread use of this reaction in biomass-to-liquid (BtL), gas-to-liquid (GtL) and coal-to-liquid (CtL) processes. Power produced by renewable energy installations is here used to provide hydrogen via electrolysis and carbon dioxide via DAC to the FT reaction. Since all these technologies are at a high level of readiness, the aim of this chapter will be to analyze their common integration and relationships in order to produce a neutral synthetic fuel, which can be used in the transportation and aviation sectors to accelerate their decarbonization.

7.1.1 FT-Process Description

Sec. A.1 already introduces the nodes necessary for the production of H_2 and CO_2. The purpose of this section is therefore to introduce the Fischer-Tropsch reaction and his integration into an RREH. The entire process is developed on Fig. 7.1

The FT process is a series of chemical reactions that can produce a variety of hydrocarbons of form $C_n\ H_{2n+2}$. The reaction is formulated such as:

$$(2n+1)H_2 + nCO \rightarrow C_nH_{2n+2} + nH_2O \qquad \Delta H = -165\ kJ/mol_{CO_2} \tag{7.1}$$

The required CO can be produced from CO_2 via the reverse water gas shift (RWGS) reaction:

$$H_2 + CO_2 \rightarrow CO + H_2O \qquad \Delta H = 42\ kJ/mol \tag{7.2}$$

The amount of H_2 required for this reaction is so low that it would be almost negligible. The RWGS reaction also produces water, which can be seen as a byproduct by the system and can be reused in the system, for example as an input for the electrolyzer.

Furthermore, the Fischer-Tropsch reaction also releases water, which can be used for the same purpose, but is also a highly exothermic process. The heat can thus be recovered to be used for the CO_2 capture. However, the previously introduced DAC does not account for a heat input. In order to modify the implementation of the technology, the techno-economic parameters from Michael Fonder et al. (2024) [25] are used to introduce a DAC utilizing available heat.

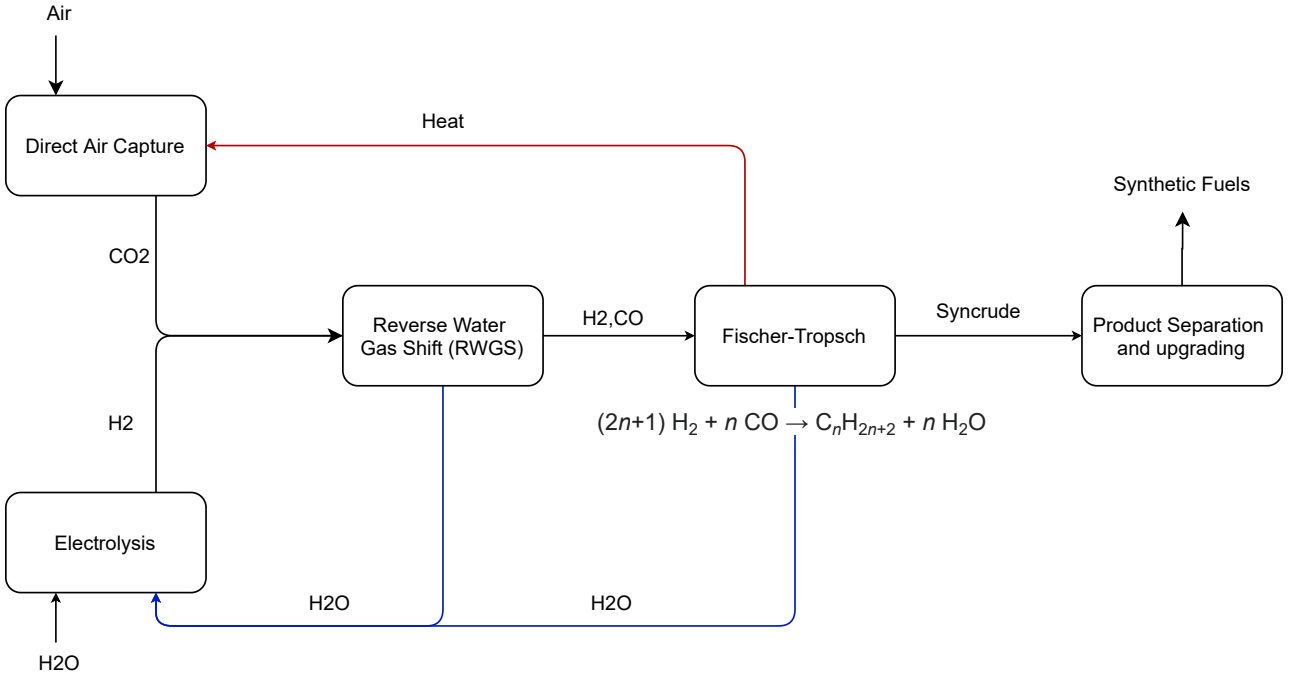

Figure 7.1: Development of the entire FT-Process including all steps: Reverse Water Gas Shift (RWGS) reaction, FT reaction and the product separation and upgrading.

The product of the FT reaction is called syncrude and consist of a mixture of hydrocarbons of various sizes, often described by their carbon number. The lightest products have fewer carbon atoms. This ranges from C1 (methane) to higher carbon chains such as C40 (tar, used for route creation for example). The mixture obtained in the syncrude heavily depends on operating conditions [52], such as the operating conditions of various components (temperature and pressure), or the types of catalysts used (iron, cobalt, etc.).

The syncrudes must be treated to obtain the desired range of products. Depending on these, different chemical steps and physical components will be necessary to achieve the desired carbon chain sizes and properties. Daniel H. König et al. (2015) [53] illustrates well all the necessary components for each step of the process. From separation units to compressors and pumps, the operating conditions of each unit are crucial to obtaining a mix of desired products.

The modeling of all these different steps of the FT process will be treated as a unique block, a node taking CO_2 and H_2 as inputs and outputting a liquid mixture of hydrocarbons called FT-Products, with techno-economic parameters that will vary the output, the implementation will be done like a black box. These different parameters will be introduced in the following section. Fig. 7.2 illustrates the integration of the node into the RREH that will be studied.

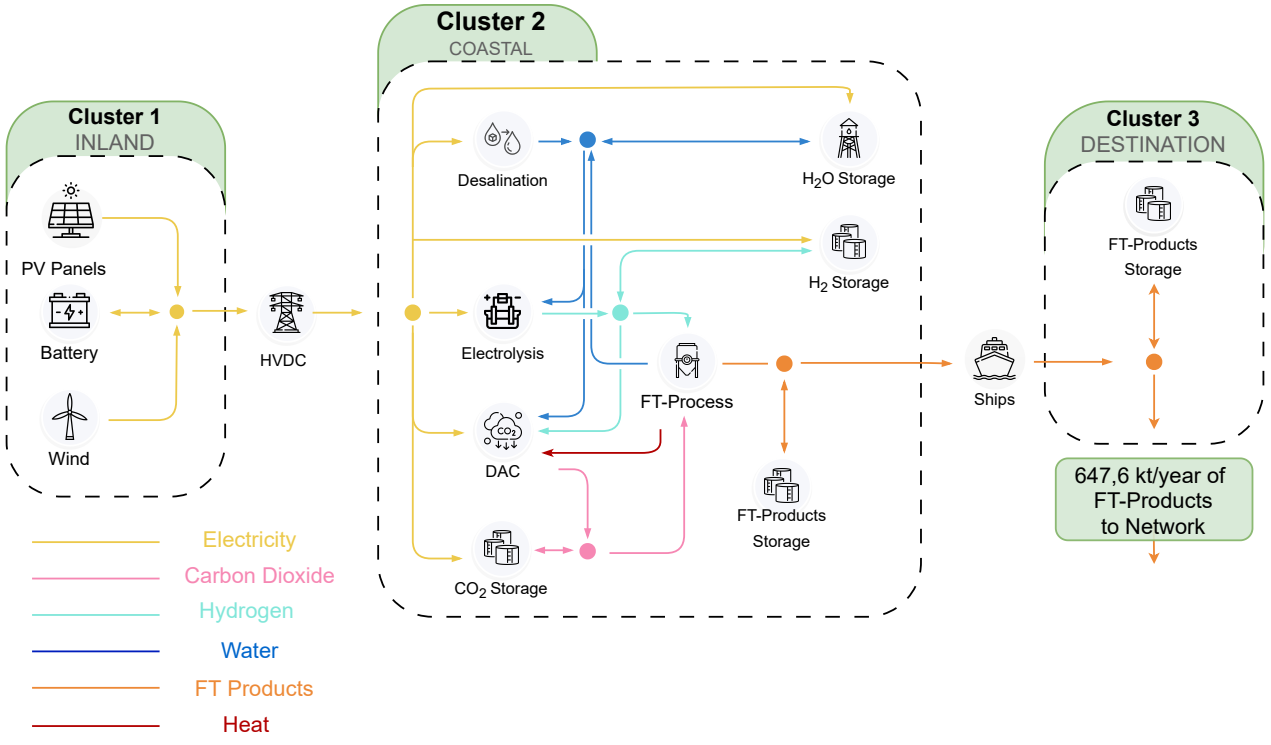

Figure 7.2: Integration of FT-Process in a RREH adapted from Berger et al. [5]. Icons symbolize conversion or storage nodes, whereas bullets and arrows schematically denote conservation hyperedges.

7.1.2 FT-products description and models

Many studies have been conducted on the pure modeling of the entire process using Aspen Plus software, allowing for the creation of complex models and their simulation. Colleli et al. (2023) [54] analyzes the economic efficiency of producing synthetic kerosene. Two main processes are studied: a two-stage indirect process and a direct process. Kinetic models are used to evaluate reactions, and sensitivity analyses are carried out to optimize costs and efficiency.

The article entitled "*Power-to-X: Modelling of Fischer-Tropsch synthesis in Aspen Plus*" [55] investigates PtX technologies and analyzes carbon-neutral FT synthesis, highlighting its large-scale feasibility, claiming carbon-neutral FT synthesis is not yet ready for large-scale production but a reduction in green hydrogen costs could make FT fuels economically competitive with their fossil equivalents. Dieterich V. et al (2020) [56] explores PtL processes that transform hydrogen and carbon dioxide into synthetic liquid fuels, offering an alternative for sectors that are difficult to decarbonize. It highlights current challenges and developments, particularly for the production of methanol, DME and Fischer-Tropsch fuels, offering avenues for future research and technological development.

However, modeling the entire process with Aspen is not within the scope of this report. Therefore, scientific literature will serve as the primary source for acquiring requisite technical parameters for desired outputs essential for constructing our FT node as a black-box.

Particular attention will be paid to the production of gasoline, diesel and kerosene, three e-fuels that can be used in the automotive, transport and aviation sectors. These fuels have the advantage of having a higher energy density than methane, previously considered. Their main characteristics are summarized in Tab. 7.1

FT-Products	Gasoline	Diesel	Kerosene
Carbon chains	C4-C12	C12-C20	C12-C18
Usage	Fuel for vehicles: cars, motorcycles, light utility vehicles	Fuel for vehicles: trucks, buses, trains, utility vehicles	Fuel for jet engines, turbojets, aircraft engines
Storage	Easy	Easy	Easy

Table 7.1: FT-Products characteristics and usage.

These fuels can all be produced from hydrogen and carbon dioxide. So what will change between a system producing more diesel or more kerosene will be the internal components of the FT-process or the operating conditions of these. These systems are taken from existing studies, in order to obtain the conversion parameters needed to obtain the input/output ratio, and therefore the quantity of each fuel for each system.

The first model to be created is based on technology of FT studied by Daniel H. König et al. (2015) [53]. The proposed configuration is aimed primarily at the production of lighter fuels, including gasoline. Then, the paper entitled *"A Techno-Economic Assessment of Fischer–Tropsch Fuels Based on Syngas from Co-Electrolysis"* from Peters R. et al (2022) [57] will be taken to target majority production of e-diesel. Finally, the last system will be more focused will be the production of kerosene with models from Atsonios K. et al. (2023) [58].

The utilization of three distinct systems, from three different studies, will give varying model parameters and subsequent configurations for the RREH. All the parameters used in the modeling are summarized in Sec. 7.2. The corresponding proportional outputs for each configuration are shown in Fig. 7.3

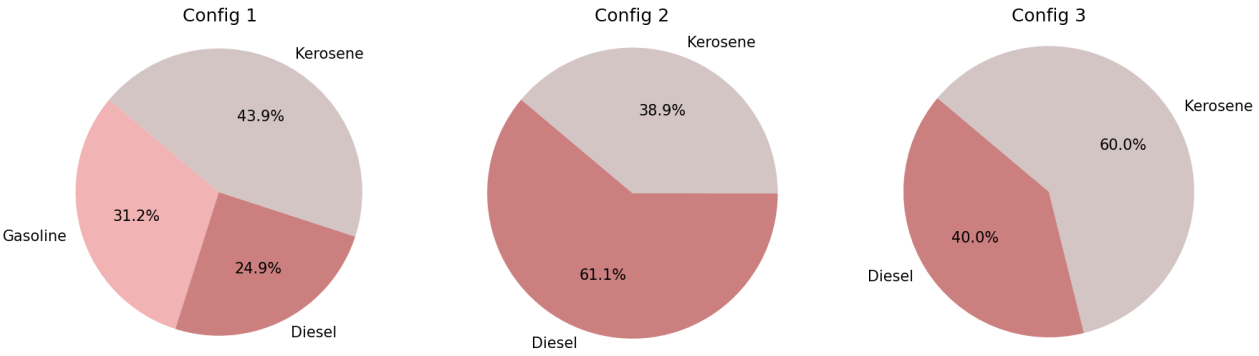

Figure 7.3: FT-Products output depending on configurations. While gasoline and diesel can be used in vehicles, kerosene is principally used in aviation sector.

In order for the different products to be used in the sectors under consideration, it is necessary that the products be of similar quality to those conventionally used. The products coming out of the FT-process are cleaner than conventional fuels because the chemical reaction is well controlled, with uniform and predictable compositions based on pure hydrogen and carbon dioxide molecules. Optimum operating conditions eliminate any impurities that may be created, whereas conventional fuels may naturally contain impurities such as sulfur or benzene [59].

However, while gasoline and diesel have mainly performance criteria that can be easily adjusted in the refinery if need be, the kerosene used in aircraft has stricter criteria to ensure the safety that is the priority in this sector. Specific standards are in place, such as the latest updated versions of British standard DEF STAN 91-091, US standard ASTM D1655 and the NATO F-35 specification. Atsonios K. et al. (2023) [58] explains in more detail how the kerosene resulting from the FT-process meets the necessary standards for synthetic fuel oil. Tab. 7.2 summarizes its characteristics and compares the values with those required, showing that most of the criteria are met, with the exception of fuel density. However, this attribute is not a major obstacle and could easily be modified, by adding additives in refinery, so it is assumed that the fuels obtained by FT are of equivalent quality to conventional fuels.

Fuel Properties	Standard A1	Synthetic Fuel
LHV [MJ/kg]	> 42.80	44.15
Density [kg/m^3]	775-840	744.3
Viscosity (-20°C) [mm^2/s]	< 8.0	5.28
Flashpoint	> 38	44.4
Distillation 10%	< 205	153.1
Distillation 100%	< 300	288.7

Table 7.2: Produced synthetic jet fuel properties compared with mandatory standards A1.

7.2 Implementation and Simulations

The FT-process node will be modeled in three distinct cases as discussed in Sec. 7.1.2, with the conversion parameters changing each time. These parameters are introduced in such a way as to produce a kiloton of FT-products each time. More concretely, if $\phi_1 = 0.519\ kt_{H_2}/kt_{FT}$ from config 3 is considered, this means that 0.519 kt of hydrogen are needed to produce one kiloton of FT-products, i.e. 0.6 kt of kerosene and 0.4 kt of diesel (according to the proportions shown in Fig. 7.3).

Conversion parameters of DAC have also been adapted so that the plant takes heat into account as an input, as discussed in Sec. 7.1.1. All the technical parameters introduced are listed in Tab. 7.3.

	ϕ_1	ϕ_2	ϕ_3	ϕ_4	μ	$\Delta_{+,-}$
FT-Process	0.547	4.16	3.3	0.06	1	0
Config 1 [53]	kt_{H_2}/kt_{FT}	kt_{CO_2}/kt_{FT}	kt_{H_2O}/kt_{FT}	kt_{heat}/kt_{FT}	-	-/h
FT-Process	0.53	3.04	3.46	0.06	1	0
Config 2 [57]	kt_{H_2}/kt_{FT}	kt_{CO_2}/kt_{FT}	kt_{H_2O}/kt_{FT}	kt_{heat}/kt_{FT}	-	-/h
FT-Process	0.519	3.417	3.21	0.06	1	0
Config 3 [58]	kt_{H_2}/kt_{FT}	kt_{CO_2}/kt_{FT}	kt_{H_2O}/kt_{FT}	kt_{heat}/kt_{FT}	-	-/h
Direct Air	0.15	5.0	0.0438	0.2	1	0
Capture [25]	GWh_{el}/kt_{CO_2}	kt_{H_2O}/kt_{CO_2}	kt_{H_2}/kt_{CO2}	GWh_{heat}/kt_{CO2}	-	-/h

Table 7.3: Technical Parameters of new nodes introduced to produce FT-Products.

An important change in the implementation of the RREH is the storage of hydrocarbons. In contrast to methane, FT-products do not require an advanced device. The liquid product coming out of the overall process can simply be stored in conventional barrels, which have basic but sufficient safety measures. Consequently, the costs associated with FT-product storage nodes will be considered negligible.

The economic parameters used to model the FT-process are taken from ElSayed M. et al. [60]. His paper investigates potential in Egypt for a transition to 100% renewable energy, exploring scenarios involving e-fuels, e-chemicals, and carbon dioxide removal technologies. The economic parameters of the DAC are once again taken from Fonder M. et al (2023) [25]. All economic parameters are listed in Tab. 7.4

	CAPEX	FOM(θ_f)	VOM(θ_v)	Lifetime
FT-Process	12407.4	6.1	0	25
[60]	$M€/(\mathrm{kt}_{FT}/h)$	$M€/(\mathrm{kt}_{FT}/h) - yr$	$M€/\mathrm{kt}_{FT}$	yr
Direct Air	6000	300	0.0	20
Capture [25]	$M€/(\mathrm{kt}_{CO2}/h)$	$M€/(\mathrm{kt}_{CO2}/h) - yr$	$M€/\mathrm{kt}_{CO2}$	yr

Table 7.4: Economical Parameters of new nodes introduced to produce FT-Products.

Finally, it is important to specify that external demand is modeled with $\lambda_t^e = 0.07393$ kt/h (see App. A.3). This gives a total of 647.6 kt/year of FT-Products to network, or approximately 7900 TWh/year. For information, the external demand for the DOC part in Chp. 4 was also equal to 647.6 kt/year.

7.2.1 FT-Products Costs and Analysis

For conducting an economic analysis and facilitating comparison with actual markets, the product pricing will be assessed in euros per kilogram, referencing the prevailing barrel or gallon prices in the American market. Subsequently, the derived objective function (refer to Eq. 3.18) in euros will be normalized by the aggregate volume of exported FT-Products.

The economic evaluation will focus on the cost of FT-products, assuming uniform prices across all hydrocarbons. This is based on the assumption that the proportion of the system that is built/used (and therefore the costs incurred) is the same as the proportion of the hydrocarbon among the FT-products. For illustration, if the total cost is €100M to produce 10 MKg of FT-Products (which is €10/kg_{FT}), with 60% being kerosene resulting in 6 Mkg, the cost for kerosene production would be the same proportion, i.e., €60M, and therefore also €10/kg.

Economic studies have already been carried out to determine the cost of producing e-fuel from Fischer-Tropsch. Delgado et al (2023) [61] uses the same technologies, but powered by nuclear energy, estimating a minimum fuel selling price of 1.08 €/kg (or 0.85 €/kg depending on configurations) of FT-products fuel mix. Pratschner S. et al. (2024) [62] have also examined a comparable system, emphasizing the characteristics of the power source, such as electricity costs and the duration of full-load operation. FT-products net production costs varied from 2.42 to 4.56 €/kg for grid-based scenarios, while off-grid scenarios yielded values ranging from 1.28 to 2.40 €/kg.

The system considered in this report therefore provides a new approach concerning the energy source. The simulations for the different configurations give costs of FT-products produced from renewable energy from 2.13 €/kg to 2.41 €/kg. Fig. 7.4 gives prices for each configuration as well as cost breakdowns for each part of the system.

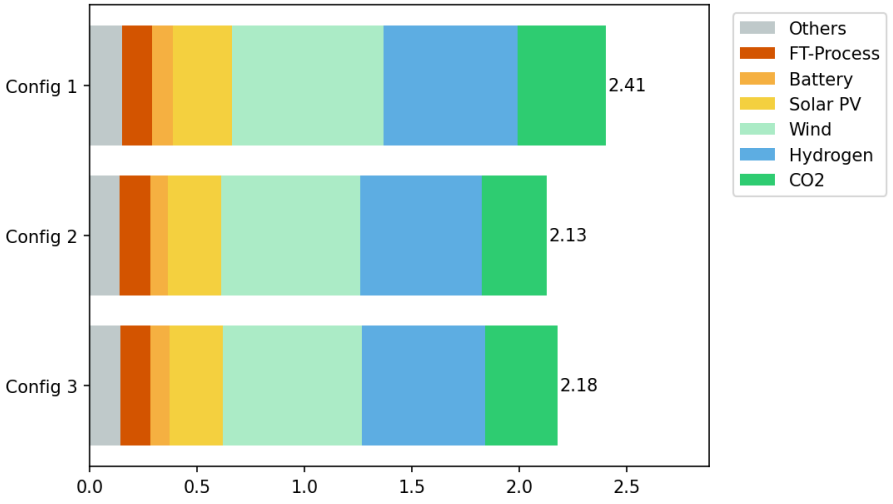

Figure 7.4: Cost breakdown comparison for each configurations in reference scenario in €/kg, with a total cost varying from 2.18 to 2.41 €/kg, as a result of technical parameters changes affecting the costs associated with each part.

The majority of costs are linked to the units of the inland cluster, those linked to electricity production. For all configurations, this corresponds to almost 50% of the cost, value which remains more or less constant for the 3 scenarios. What makes the cost vary depending on the configurations are the parts related to the units and products necessary for the FT-process, namely the electrolyzer and the DAC. A slight change in the conversion parameters is enough for the quantities of H_2 and CO_2 to be produced to increase considerably, leading to a further increase in the installed capacity of the units producing them, and the associated costs, which in turn up the price.

Costs are higher for configuration 1 because the conversion parameters are the most disadvantageous, logically increasing the installed capacity needed to meet demand. Fig. 7.5 illustrates the differences in installed capacity between each configuration showing that a change in the technical parameters of a single unit varies the installed capacities of many units.

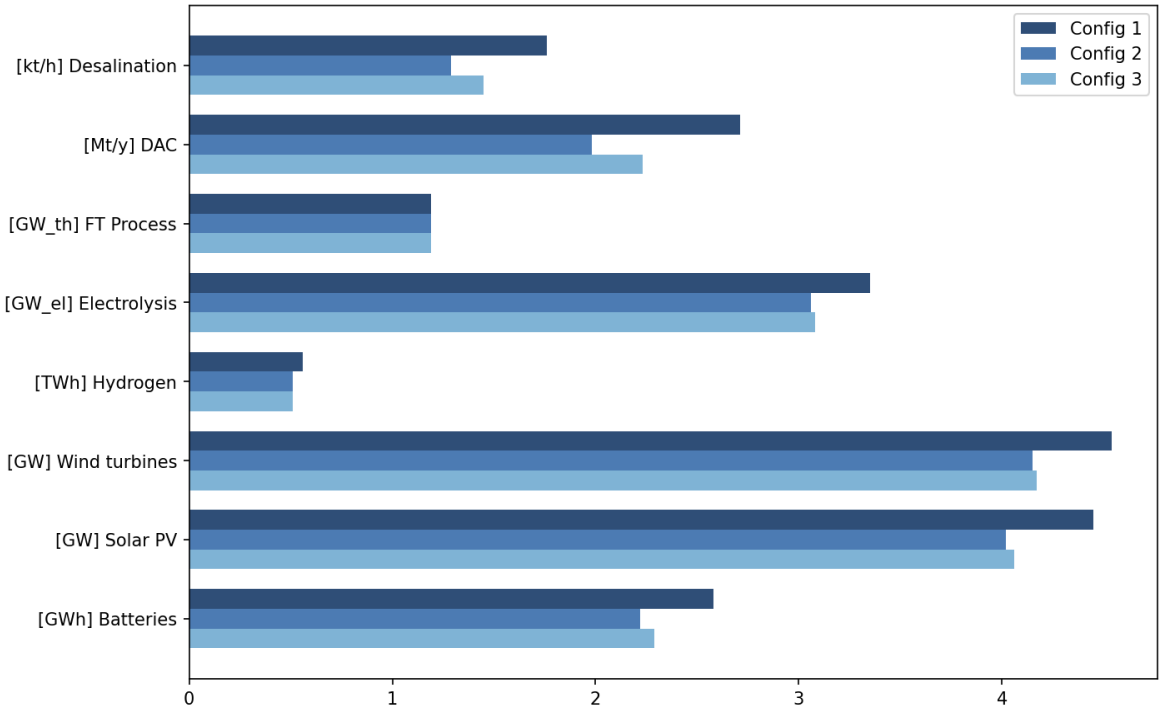

Figure 7.5: Installed capacities comparison of important plants for each configurations in reference scenario, showing that change in technical parameters for one unit can result in multiple modifications to the system.

7.2.2 Sensitivity Analysis

The sensitivity analysis investigates the impact of changes in techno-economic parameters on FT-product costs. The different configurations used for the simulations were in fact a partial analysis, by changing the FT-process conversion parameters. Here, the techno-economic parameters will again be changed at FT-process level, but in a similar way for each configuration, in order to maintain the different initial ranges. This means that the parameters will be 20% worse in the conservative scenario, and 20% better in the optimistic case. These ratios, which have been defined on the basis of the expertise acquired during the literature review, will be applied to CAPEX, VOM, FOM and conversion parameters ϕ_1 and ϕ_2 of the FT-process plant.

Simulating the three configurations in the three possible scenarios - optimistic, reference or conservative - gives new costs ranging from 1.69 to 2.90 €/kg. Fig. 7.6 summarizes the costs for each configuration in each scenario.

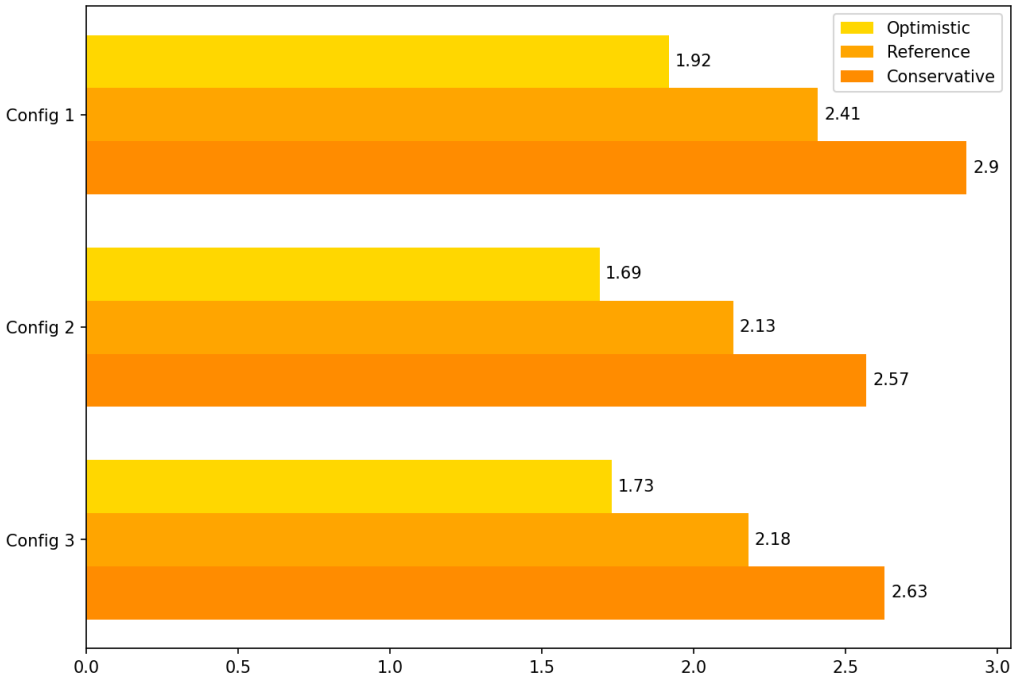

Figure 7.6: Cost Breakdown Comparison for each configurations in reference, optimistic or conservative scenario in €/kg, with a total cost varying from 1.69 €/kg in config 2 with optimistic scenario to 2.9 €/kg in config 1 with conservative scenario.

One of the direct causes of the consequent changes between the prices of the different scenarios is the installed capacity of DAC, which results from an increased need for CO2 due to unfavorable conversion parameters in some cases. The worst price, configuration 1 in the conservative scenario has 3.25 Mt/y of installed DAC while the best configuration in the optimistic scenario is at 1.58 Mt/y of DAC, which is more than half.

7.2.3 Influence of electrolyzer technology

The aim of this section is to study the impact of technical changes on the electrolyzer plant, to see what consequences this would have on cost. As discussed in Sec. 7.1, the electrolysis technology considered is the same as in the research by Berger et al. [5] but most studies of e-fuel production via Fischer-Tropsch have used solid oxide electrolyzer cell (SOEC) technology. In contrast to conventional electrolysis technologies, the SOEC can use heat as a parallel input of electricity, reducing normal electricity consumption [63]. This allows for higher efficiency yields than conventional technologies, but is less mature and is still in the early stage of commercialization.

The fact that the SOEC suits well with the FT-process is that the reaction is highly exothermic. While heat has already been implemented as output for DAC input, it can also be added as input for electrolysis. Here, we will only consider a range of efficiencies achievable by the electrolysis node assuming that the rejected heat is sufficient to achieve higher efficiencies. The hypothesis made here is that the amount of heat released by the FT-process is such that it can achieve a maximum efficiency of 85% for the electrolysis plant.

While the reference efficiency is around 63%, simulations will be made for efficiency values ranging from 50 to 85%. While the range below 70% refers to PEM technologies, the part above designates SOEC. Fig. 7.7 shows the difference between the two ranges and the cost of FT-products as a function of electrolysis efficiency for configuration 2 in the reference scenario.

The cost varies from 2.59 €/kg for an efficiency of 50% to 1.79 €/kg for the maximal efficiency, with a non-linear relationship. Better efficiency leads to less installed capacity in power generation, which was a significant share of total costs.

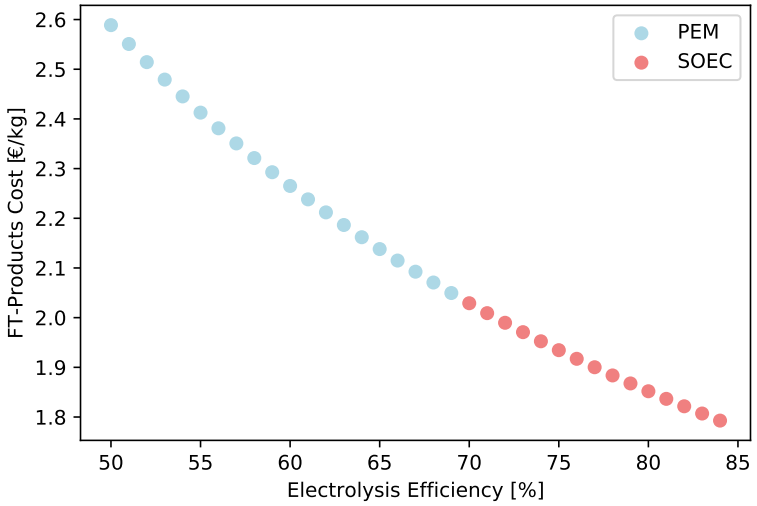

Figure 7.7: FT-products cost according to electrolyzer efficiency, showing a non-linear relationship. High efficiencies refer to SOEC (red points) technology while lower efficiencies relate to PEM technology (blue points).

Chapter 8

Conclusion

The aim of this report was to create energy systems for carbon-neutral synthetic fuel production. In particular, the implementation and optimization of Remote Renewable Energy Hubs including new technologies or concepts has been carried out in order to perform techno-economic analyses on synthetic fuel production.

After establishing the context and framework for this work, the first technology implemented was the Direct Ocean Capture, capturing carbon dioxide from water, which replaces Direct Air Capture. Its implementation reduces the total cost of the system from 149 €/MWh to 145.3 €/MWh for a system supplying 10 TWh annually of synthetic methane. Making his usage flexible over time reduces costs by up to 137 €/MWh. This technology is therefore theoretically promising, but data found has to comply with practical conditions.

The model was then adapted to suit an external water demand as well as methane demand. Water was considered as a by-product that could serve the local regions of the RREH. Its price was derived on the basis of the proportion of the system serving this demand, with a reference price of 3.64 €/t. By improving configurations, either by adapting the operating conditions of the desalination plant or by optimizing water demand, prices can be reduced from 2.92 €/t to 2.63 €/t, an excellent result compared to European standards of around 2.5 €/t.

The multi-hub concept introduced travel costs and Cap Horn, a high-potential location for an RREH with a methane price of 129.7 €/MWh. Despite these interesting points, the main goal of the chapter was not achieved, as no natural interactions were possible between different RREHs. A large future work would be to rethink how to optimize the models, with the aim of capturing interactions between hubs using more complex models.

Finally, the production of synthetic conventional fuels is attractive, given its potential for valorization in major transport sectors. Costs between 2.13 €/kg and 2.41 €/kg are obtained for production of gasoline, diesel and kerosene via the Fischer-Tropsch reaction. An optimistic scenario shows costs falling to 1.69 €/kg. The results are equivalent to those obtained in the scientific literature and are not much higher than conventional fuels. These findings are promising, but they primarily stem from preliminary scientific investigations. Constructing models in thermodynamics equation solver could enhance this section, providing precise product proportions, conversion factors, and heightened quality assurances.

Appendix A

System configuration and parameters

A.1 Conversion nodes

This subsection comprises detailed explanations for each conversion node, accompanied by tables displaying the associated technical and economic parameters used to model them. The data used are estimates for 2030.

Solar photovoltaic panels are used for power generation. To realistically model the system, capacity factors π_t^n of irradiance data were obtained from the ERA5 database [68] over a 5 year period (2015-2019) and averaged to predict future weather conditions with a degree of certainty (See Fig. A.3). When selecting the locations for PV panels, a choice was made based on the quality of the capacity factor, as depicted in Fig. 2.3 The plant is modeled with an external variable being the output power production and an internal variable representing the installed capacity.

Wind turbines are also used for power generation. Similarly to solar, wind speed capacity factors π_t^n are retrieved from the ERA5 database [68] over the period 2015-2019 and also averaged to select the best capacity factors for choosing the locations of installations, as illustrated in Fig. 2.3. The only external and internal variables are respectively the output power and the capacity.

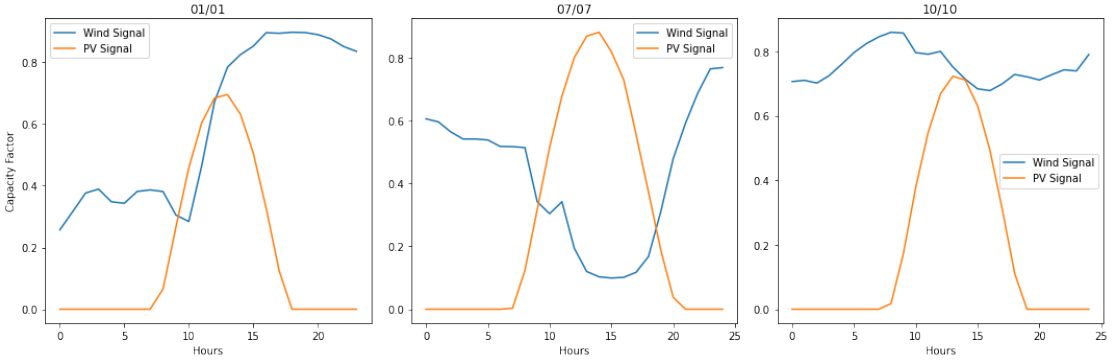

Figure A.1: Sample of capacity factor π_t^n.

High voltage direct current (HVDC) ensures the transmission of power between the inland and coastal clusters. Since both means of production are in close proximity, the transmission line is located right next to them and is assumed to be directly connected, making the infrastructure costs connecting them negligible. The assumed 1000 km-long line utilizes two voltage source converters at each end station and get a power loss of 1.8%. The transmission-related loss is 1.5% of the power, resulting in a total efficiency as presented in Tab. A.1. The node has two external variables, which are the in and outgoing power, while the internal variable is the line capacity.

Water desalination plant's purpose is to produce fresh water from seawater. To achieve this, the conventional technology, reverse osmosis, is utilized. This process involves the use of a semi-permeable membrane to remove impurities and contaminants from water by forcing it through the membrane under high constant pressure. The plant requires electricity to produce fresh water, which serves as the two external variables. The internal variable, capacity, is referenced in relation to water. Seawater is not considered as an input, as it is assumed to be freely accessible, and the cost of obtaining it is negligible. The membranes have the mechanical constraint of operating continuously, which is one of the parameters listed in Tab. A.1.

Electrolysis plant split fresh water into hydrogen and oxygen using proton exchange membrane, powered by an electric current and operating at 20 bar and 40°C. This results in a total of 4 external variables: water, electricity, oxygen, and hydrogen which is the reference commodity. The internal variable, capacity, is sized in relation to the power input. The plant has mechanical particularities, such as a minimum level of hydrogen output when it is operational, as well as the ability to be flexible and ramp up and down very quickly. All of these parameters are listed in Tab. A.1.

Direct Air Capture units enable the extraction of CO2 from natural air. A unit is based on two chemical loops. The first loop employs aqueous sorbents to capture carbon dioxide from the air, converting it into dissolved compounds and then into solid compounds. The second loop retrieves the carbon dioxide by calcining the solid compounds and replenishing the sorbents, requiring electricity to power the system components. The various loops also require hydrogen to generate heat and fresh water to create aqueous solutions, all in order to produce gaseous CO2. This results in a total of 4 external variables. The different conversion parameters are detailed in Tab.A.1, with the reference flow being the carbon dioxide output. Capacity is the only internal variable.

	ϕ_1	ϕ_2	ϕ_3	μ	$\Delta_{+,-}$
HVDC Interconnection	0.9499				
	-				
Desalination	0.004			1.0	0.0
	GWh_{el}/kt_{H_20}			-	-/h
Electrolysis	50.6	9.0	8.0	0.05	1.0
	GWh_{el}/kt_{H_2}	kt_{H_2O}/kt_{H_2}	kt_{O_2}/kt_{H_2}	-	-/h
Methanation	0.5	2.75	2.25	1.0	0.0
	kt_{H_2}/kt_{CH_4}	kt_{CO_2}/kt_{CH_4}	kt_{H_2O}/kt_{CH_4}	-	-/h
Direct Air Capture	0.1091	0.0438	5.0	1.0	0.0
	GWh_{el}/kt_{CO_2}	kt_{H_2}/kt_{CO_2}	kt_{H_2O}/kt_{CO_2}	-	-/h
CH_4 Liquefaction	0.616			0.0	1.0
	GWh_{el}/kt_{LCH4}			-	-/h
LCH_4 Carriers	0.994				
	-				
LCH_4 Regasification	0.98				
	-				

Table A.1: Technical parameters of conversion nodes from Berger et al. [5].

Methanation plants has four external variables. Indeed, carbon dioxide and hydrogen are used in stoichiometric proportions to produce gaseous methane and water vapor through the highly exothermic Sabatier reaction. The reference flow is methane, which is also used to size the plant, making capacity the only internal variable. To maintain high-quality production, the plant is assumed to operate in steady-state. The various technical parameters are detailed in Tab. A.1.

Methane liquefaction units allow for the conversion of gaseous methane into liquid form through several stages of compressors and pumps, powered by electricity, using the Joule-Thomson effect. This results in 3 external variables: electricity, gaseous methane, and liquid methane as the reference flow. The plant's capacity is the internal variable, and the parameters are detailed in Tab. A.1.

Methane carriers transport liquid methane from the coastal cluster to Europe, and the advantage is that they can use the same methane they are transporting as fuel. This results in a conversion parameter detailed in Tab. A.3, with fairly high efficiency. External variables are the coastal methane and the methane reaching its destination while the internal variable is the carrier capacity. The journey is modeled with Eq. 3.3, providing the parameter $\tau_i^n = 116$h. 7 identical carriers making round trips are considered, with loading and unloading taking 24 hours, and their schedules not overlapping in any way.

Regasification units only utilizes two external variables: the incoming liquid methane and the produced gaseous methane. This assumption is made to avoid using electricity for heat production during the reaction. Instead, 2% of the total methane is used to provide the required heat, resulting in a high conversion parameter. The capacity, the only internal variable, is based on the methane level.

	CAPEX	FOM(θ_f)	VOM(θ_v)	Lifetime
Solar PV Panels	380.0	7.25	0.0	25.0
	$M€/\mathrm{GW}_{el}$	$M€/\mathrm{GW}_{el} - yr$	$M€/\mathrm{GWh}_{el}$	yr
Wind Turbines	1040.0	12.6	0.00135	30.0
	$M€/\mathrm{GW}_{el}$	$M€/\mathrm{GW}_{el} - yr$	$M€/\mathrm{GWh}_{el}$	yr
HVDC Interconnection	480.0	7.1	0.0	40.0
	$M€/\mathrm{GW}_{el}$	$M€/\mathrm{GW}_{el} - yr$	$M€/\mathrm{GWh}_{el}$	yr
Electrolysis	600.0	30.0	0.0	15.0
	$M€/\mathrm{GW}_{el}$	$M€/\mathrm{GW}_{el} - yr$	$M€/\mathrm{GWh}_{el}$	yr
Methanation (HHV)	735.0	29.4	0.0	20.0
	$M€/\mathrm{GW}_{CH_4}$	$M€/\mathrm{GW}_{CH_4} - yr$	$M€/\mathrm{GWh}_{CH_4}$	yr
Desalination	28.08	0.0	0.000315	20.0
	$M€/(\mathrm{kt}_{H_2O}/h)$	$M€/(\mathrm{kt}_{H_2O}/h) - yr$	$M€/\mathrm{kt}_{H_2O}$	yr
Direct Air Capture	4801.4	0.0	0.0207	30.0
	$M€/(\mathrm{kt}_{CO_2}/h)$	$M€/(\mathrm{kt}_{CO_2}/h) - yr$	$M€/\mathrm{kt}_{CO_2}$	yr
CH_4 Liquefaction	5913.0	147.825	0.0	30.0
	$M€/(\mathrm{kt}_{LCH_4}/h)$	$M€/(\mathrm{kt}_{LCH_4}/h) - yr$	$M€/\mathrm{kt}_{LCH_4}$	yr
LCH_4 Carriers	2.537	0.12685	0.0	30.0
	$M€/\mathrm{kt}_{LCH_4}$	$M€/\mathrm{kt}_{LCH_4} - yr$	$M€/\mathrm{kt}_{LCH_4}$	yr
LCH_4 Regasification	1248.3	24.97	0.0	30.0
	$M€/(\mathrm{kt}_{CH_4}/h)$	$M€/(\mathrm{kt}_{CH_4}/h) - yr$	$M€/\mathrm{kt}_{CH_4}$	yr

Table A.2: Economic parameters of conversion nodes from Berger et al. [5].

A.2 Storage nodes

Storage nodes are described here along with the tables containing the techno-economic data (2030 estimates).

Lithium-ion battery storage are used for short-term electricity storage. Power in/outflows are the external variables while the power capacity and the level of charge are internal variables. Techno-economical parameters are situated in Tabs. A.3, A.4, A.5 and A.6 for all nodes.

	η^S	η^+	η^-	σ	ρ	ϕ
Battery Storage	0.00004	0.959	0.959	0.0	1.0	
	-	-	-	-	-	
Compressed H_2 Storage	1.0	1.0	1.0	0.05	1.0	1.3
	-	-	-	-	-	GWh_{el}/kt_{H_2}
Liquefied CO_2 Storage	1.0	1.0	1.0	0.0	1.0	0.105
	-	-	-	-	-	GWh_{el}/kt_{CO_2}
Liquefied CH_4 Storage	1.0	1.0	1.0	0.0	1.0	
	-	-	-	-	-	
H_2O Storage	1.0	1.0	1.0	0.0	1.0	0.00036
	-	-	-	-	-	GWh_{el}/kt_{H_2O}

Table A.3: Technical parameters of storage nodes from Berger et al. [5].

Hydrogen storage tanks maintain the gas under pressure, which, arriving directly from the electrolysis unit at 20 bars, must be increased to 200 bars using electrically powered compressors. So, the three external variables are electricity, and the in/outflow of hydrogen. The three internal variables are the level of charge, the power capacity, and the energy capacity. Also, tanks must have 5% of minimum inventory level.

Water storage tanks are conventional technologies with electrically powered pumps. Three external variables are power consumption and water in/outflows and the three internal variables are the level of charge, the flow of water (the size of the pipes connecting the tanks) and the installed capacity.

Liquefied methane storage tanks are designed in a way that prevents any leaks such that efficiency is 100%. Also, the electrical consumption used to keep the methane properly liquefied is negligible. There is therefore two external variables with the in/outflows of liquid methane and internal variables are state of charge and the tank capacity.

	η^S	η^+	η^-	σ	ρ	ϕ
Battery Storage	0.00004	0.959	0.959	0.0	1.0	
	-	-	-	-	-	
Compressed H_2 Storage	1.0	1.0	1.0	0.05	1.0	1.3
	-	-	-	-	-	GWh_{el}/kt_{H_2}
Liquefied CO_2 Storage	1.0	1.0	1.0	0.0	1.0	0.105
	-	-	-	-	-	GWh_{el}/kt_{CO_2}
Liquefied CH_4 Storage	1.0	1.0	1.0	0.0	1.0	
	-	-	-	-	-	
H_2O Storage	1.0	1.0	1.0	0.0	1.0	0.00036
	-	-	-	-	-	GWh_{el}/kt_{H_2O}

Table A.4: Technical parameters of storage nodes from Berger et al. [5].

Liquefied carbon dioxide storage tanks also use liquefaction and regasification units to store carbon dioxide. Liquefaction is done using electricity while regasification use ambient air to recover gaseous CO_2. Therefore, there are 3 external variables, including the in/outflow of carbon dioxide and the electrical consumption for liquefaction, and 5 internal variables, including the level of charge, flows of liquefied CO_2, the tank capacity and capacities of both liquefaction and regasification units.

	CAPEX	FOM(θ_f)	VOM(θ_v)	Lifetime
Battery Storage	142.0	0.0	0.0018	10.0
	M€/GWh	M€/GWh-yr	M€/GWh	yr
Compressed H_2 Storage	45.0	2.25	0.0	30.0
	M€/kt	M€/kt-yr	M€/kt	yr
Liquefied CO_2 Storage	1.35	0.0675	0.0	30.0
	M€/kt	M€/kt-yr	M€/kt	yr
Liquefied CH_4 Storage	2.641	0.05282	0.0	30.0
	M€/kt	M€/kt-yr	M€/kt	yr
H_2O Storage	0.065	0.0013	0.0	30.0
	M€/kt	M€/kt-yr	M€/kt	yr

Table A.5: Economic parameters of storage nodes (stock component) from Berger et al. [5].

	CAPEX	FOM(θ_f)	VOM(θ_v)	Lifetime
Battery Storage	160.0	0.5	0.0	10.0
	M€/GW	M€/GW-yr	M€/GWh	yr
Liquefied CO_2 Storage	48.6	2.43	0.0	30.0
	M€/(kt/h)	M€/(kt/h)-yr	M€/kt	yr
H_2O Storage	1.55923	0.0312	0.0	30.0
	M€/(kt/h)	M€/(kt/h)-yr	M€/kt	yr

Table A.6: Economic parameters of storage nodes (flow component) from Berger et al. [5].

A.3 Conservation Hyperedges

Hyperedges are introduced here to maintain continuity between different nodes. It will be assumed that λ_t^e is zero for all cases, except as noted, indicating that there is no exogenous power injection or withdrawal.

Inland power balance use the Kirchhoff law such that the sum of power flows from PV panels, wind turbines and batteries outflow is equal to the sum of power for the battery inflow and HVDC connection. As with all storage nodes, it is ensured that the charging and discharging of units do not occur simultaneously.

Coastal power balance ensures that the HVDC provides the necessary power to the units in the coastal cluster, which are the desalination plant, the direct air capture, the electrolysis plant, the hydrogen and water storage, the methane liquefaction units and the liquefied CO_2 storage.

Coastal hydrogen balance enforces the mass flow conservation between the sum of hydrogen storage unit outflow and electrolysis plant with the sum of flows for direct air capture plant, methanation unit and the storage system inflow.

Coastal carbon dioxide balance ensures the mass flow conservation, the sum of flows from the direct air capture and the storage outflow must be equal to the sums of flows to methanation plant and the storage unit inflow.

Coastal water balance maintains equality between the masses of fresh water coming from one side of the desalination unit and the outputs of the storage tanks, and on the other side, the inputs of the electrolysis plant, direct air capture, and the storage unit. Eq. 3.19 can be relaxed to "greater than or equal" because water can be released into the environment (or for other uses) in case of overproduction.

Coastal methane balance guarantees conservation of gaseous mass flow from methanation plant to liquefaction unit.

Coastal liquefied methane balance enforces the liquid mass flow conversation between the sum of flows from the liquefaction unit and the storage outflow and the sum of flows to methane carriers and storage system inflow.

Destination liquefied methane balance ensures the conservation of liquefied methane mass flow. The sum of flows from methane carriers discharge and the storage output must be equal to the flows of regasification units and storage system inflow.

Destination methane balance enforces that the regasification plant satisfies the methane gas demand, which is 10 TWh (HHV) per year. That being said, no assumptions are made regarding the future use of this energy, which can be used as it is or converted into electricity. It is assumed that synthetic methane has a HHV of 15.441 kWh/kg and that the profile demand is constant for every t such that the exogenous demand is

$$\lambda_t^e = 10 \times \frac{10^3}{8760} \times \frac{1}{15.441} = 0.07393\text{kt/h}$$

Bibliography

[1] Sorrell, Steve. ■ Reducing energy demand: A review of issues, challenges and approaches ■. Renewable and Sustainable Energy Reviews, vol. 47, July 2015, p. 74-82. ScienceDirect, https://doi.org/10.1016/j.rser.2015.03.002

[2] Berger, Mathias, et al. ■ The role of power-to-gas and carbon capture technologies in cross-sector decarbonisation strategies ■. Electric Power Systems Research, vol. 180, March 2020, p. 106039. ScienceDirect, https://doi.org/10.1016/j.epsr.2019.106039

[3] Dachet, Victor, et al. Remote Renewable Energy Hubs (V2). 2023. orbi.uliege.be, https://orbi.uliege.be/handle/2268/306582

[4] Miftari, Bardhyl et al. (2022). "GBOML: Graph-Based Optimization Modeling Language". In: Journal of Open Source Software 7.72, p. 4158https://gboml.readthedocs.io/en/latest/

[5] Berger, Mathias, et al. ■ Remote Renewable Hubs for Carbon-Neutral Synthetic Fuel Production ■. Frontiers in Energy Research, vol. 9, 2021. Frontiers, https://www.frontiersin.org/articles/10.3389/fenrg.2021.671279

[6] Larbanois, Antoine, et al. Ammonia, Methane, Hydrogen and Methanol Produced in Remote Renewable Energy Hubs: A Comparative Quantitative Analysis. 2023. orbi.uliege.be, https://orbi.uliege.be/handle/2268/310172

[7] Renewable Energy Targets. https://energy.ec.europa.eu/topics/renewable-energy/renewable-energy-directive-targets-and-rules/renewable-energy-targets_en

[8] EU Overachieves 2020 Renewable Energy Target. https://ec.europa.eu/eurostat/web/products-eurostat-news/-/ddn-20220119-1

[9] ■ Energy Statistics Data Browser – Data Tools ■. IEA, https://www.iea.org/data-and-statistics/data-tools/energy-statistics-data-browser

[10] Radu, David, et al. ■ Complementarity assessment of south Greenland katabatic flows and West Europe wind regimes ■. Energy, vol. 175, mai 2019, p. 393-401. ScienceDirect, https://doi.org/10.1016/j.energy.2019.03.048

[11] Fasihi, M., Bogdanov, D., and Breyer, C. (2015). "Economics of global LNG trading based on hybrid PV-wind power plants," in Proceedings of the 31st European Photovoltaic Solar Energy Conference (Hamburg), 3051–3067. doi: 10.4229/EUPVSEC20152015-7DO.15.6

[12] Three Gorges Project. https://www.ctg.com.cn/en/our_business/hydropower88/807478/index.html

[13] Hornsea 1 Offshore Wind Farm. https://orsted.co.uk/energy-solutions/offshore-wind/our-wind-farms/hornsea1

[14] Alassi, Abdulrahman, et al. ■ HVDC Transmission: Technology Review, Market Trends and Future Outlook ■. Renewable and Sustainable Energy Reviews, vol. 112, September 2019, p. 530-54. ScienceDirect, https://doi.org/10.1016/j.rser.2019.04.062

[15] Jones, Phil S., et Colin C. Davidson. ■ Calculation of power losses for MMC-based VSC HVDC stations ■. 2013 15th European Conference on Power Electronics and Applications (EPE), 2013, p. 1-10. IEEE Xplore, https://doi.org/10.1109/EPE.2013.6631955

[16] Chatzivasileiadis, S., Ernst, D., et al. ■ The Global Grid ■. Renewable Energy, vol. 57, September 2013, p. 372-83. ScienceDirect, https://doi.org/10.1016/j.renene.2013.01.032

[17] Palys, Matthew J., et Prodromos Daoutidis. ■ Power-to-X: A review and perspective ■. Computers & Chemical Engineering, vol. 165, September 2022, p. 107948. ScienceDirect, https://doi.org/10.1016/j.compchemeng.2022.107948

[18] Abdelshafy, Alaaeldin M., et al. ■ Optimal design of a grid-connected desalination plant powered by renewable energy resources using a hybrid PSO–GWO approach ■. Energy Conversion and Management, vol. 173, October 2018, p. 331-47. ScienceDirect, https://doi.org/10.1016/j.enconman.2018.07.083

[19] Chapman, A. J., Fraser, T., and Itaoka, K. (2017). Hydrogen import pathway comparison framework incorporating cost and social preference: case studies from Australia to Japan. Int. J. Energy Res. 41, 2374–2391. https://onlinelibrary.wiley.com/doi/10.1002/er.3807

[20] Poncelet, Kris, et al. ■ Impact of the level of temporal and operational detail in energy-system planning models ■. Applied Energy, vol. 162, January 2016, p. 631-43. ScienceDirect, https://doi.org/10.1016/j.apenergy.2015.10.100

[21] Dachet, Victor, et al. ■ Towards CO2 valorization in a multi remote renewable energy hub framework ■. 36th International Conference on Efficiency, Cost, Optimization, Simulation and Environmental Impact of Energy Systems (ECOS 2023),https://arxiv.org/abs/2303.09454

[22] Lambin, Clara, et al. ■ Assessment of future wind speed and wind power changes over South Greenland using the MAR regional climate model ■. International Journal of Climatology, August 2022. orbi.uliege.be, https://doi.org/10.1002/joc.7795

[23] Radu, David-Constantin, et al. ■ Complementarity Assessment of South Greenland Katabatic Flows and West Europe Wind Regimes ■. Energy, vol. 175, May 2019. orbi.uliege.be, https://doi.org/10.1016/j.energy.2019.03.048

[24] TES and University of Liège to Complete First Joint Research on ■ e-NG for Closing the Carbon Loop from Morocco to Belgium ■. 31 October 2023, https://urlz.fr/qbhE

[25] Fonder, Michaël, et al. ■ Synthetic Methane for Closing the Carbon Loop: Comparative Study of Three Carbon Sources for Remote Carbon-Neutral Fuel Synthetization ■ October 2023. orbi.uliege.be, https://orbi.uliege.be/handle/2268/307481

[26] Zeebe, R. E. & Wolf-Gladrow, D. CO2 in Seawater: Equilibrium, Kinetics, Isotopes (Elsevier, 2001)

[27] Jayarathna, Chameera, et al. ■ Review on Direct Ocean Capture (DOC) Technologies ■. SSRN Electronic Journal, 2022. DOI.org (Crossref), https://doi.org/10.2139/ssrn.4282969

[28] Pearson, Gavin. ■ Canada Set for World's Largest Offshore Carbon Capture Project ■. Infrastructure Global, 24 juillet 2023, https://infra.global/canada-set-for-worlds-largest-offshore-carbon-capture-project/

[29] ■ Technology ■. Captura, https://capturacorp.com/technology/. Consulted the 6 February 2024.

[30] Eisaman, Matthew D., et al. ■ CO2 Extraction from Seawater Using Bipolar Membrane Electrodialysis ■. Energy Environmental Science, vol. 5, no 6, 2012, p. 7346. DOI.org (Crossref), https://doi.org/10.1039/c2ee03393c

[31] Yan, Litao, et al. ■ An Electrochemical Hydrogen-Looping System for Low-Cost CO 2 Capture from Seawater ■. ACS Energy Letters, vol. 7, no 6, juin 2022, p. 1947-52. DOI.org (Crossref), https://doi.org/10.1021/acsenergylett.2c00396

[32] Digdaya, Ibadillah A., et al. ■ A Direct Coupled Electrochemical System for Capture and Conversion of CO2 from Oceanwater ■. Nature Communications, vol. 11, no 1, septembre 2020, p. 4412. www.nature.com, https://doi.org/10.1038/s41467-020-18232-y.

[33] Digdaya, Ibadillah A., et al. "Supplementary Information, A Direct Coupled Electrochemical System for Capture and Conversion of CO2 from Oceanwater", https://static-content.springer.com/esm/art%3A10.1038%2Fs41467-020-18232-y/MediaObjects/41467_2020_18232_MOESM1_ESM.pdf

[34] Zhao, Xiaoling, et al. ■ Technical and Economic Demands of HVDC Submarine Cable Technology for Global Energy Interconnection ■. Global Energy Interconnection, vol. 3, no 2, avril 2020, p. 120-27. DOI.org (Crossref), https://doi.org/10.1016/j.gloei.2020.05.004

[35] Brooks, Daniel L., et Mahendra Patel. ■ Panel: Standards & interconnection requirements for wind and solar generation NERC Integrating Variable Generation Task Force ■. 2011 IEEE Power and Energy Society General Meeting, IEEE, 2011, p. 1-3. DOI.org (Crossref), https://doi.org/10.1109/PES.2011.6039360.

[36] Mekonnen, Mesfin M., et Arjen Y. Hoekstra. ■ Four Billion People Facing Severe Water Scarcity ■. Science Advances, vol. 2, no 2, February 2016, p. e1500323. DOI.org (Crossref), https://doi.org/10.1126/sciadv.1500323

[37] THE 17 GOALS | Sustainable Development. https://sdgs.un.org/goals

[38] UN Water. Sustainable Development Goal 6: Synthesis Report 2018 on Water and Sanitation. United Nations, 2018

[39] ■ La consommation d'eau domestique est-elle la même à travers le monde? | Centre d'information sur l'eau ■. 8 February 2017, https://www.cieau.com/le-metier-de-leau/ressource-en-eau-eau-potable-eaux-usees/la-consommation-deau-domestique-est-elle-la-meme-a-travers-le-monde/

[40] Algeria Population (2023) - Worldometer. https://www.worldometers.info/world-population/algeria-population/ Accessed on 10 December 2023

[41] Groundwater, Making the Invisible Visible | UN World Water Development Report 2022. 14 février 2022, https://www.unesco.org/reports/wwdr/2022/en

[42] ■ The Global Status of Desalination: An Assessment of Current Desalination Technologies, Plants and Capacity ■. Desalination, vol. 495, décembre 2020, p. 114633. www.sciencedirect.com, https://doi.org/10.1016/j.desal.2020.114633

[43] Soliman, Mariam N., et al. ■ Energy consumption and environmental impact assessment of desalination plants and brine disposal strategies ■. Process Safety and Environmental Protection, vol. 147, mars 2021, p. 589-608. ScienceDirect, https://doi.org/10.1016/j.psep.2020.12.038

[44] Aumesquet-Carreto, Miguel-Ángel, et al. ■ Opportunities of Reducing the Energy Consumption of Seawater Reverse Osmosis Desalination by Exploiting Salinity Gradients ■. Membranes, vol. 12, no 11, November 2022, p. 1045. https://doi.org/10.3390/membranes12111045

[45] Tsai, Shao-Chi, et al. ■ Evaluation of the Specific Energy Consumption of Sea Water Reverse Osmosis Integrated with Membrane Distillation and Pressure–Retarded Osmosis Processes with Theoretical Models ■. Membranes, vol. 12, no 4, April 2022, p. 432. https://doi.org/10.3390/membranes12040432

[46] Anele, Amos, et al. ■ Predictive Uncertainty Estimation in Water Demand Forecasting Using the Model Conditional Processor ■. Water, vol. 10, no 4, April 2018, p. 475. DOI.org (Crossref), https://doi.org/10.3390/w10040475

[47] ■ Prix m3 eau Europe: comparaison Belgique et Europe ■. CallMePower, 16 May 2023, https://callmepower.be/fr/eau/prix/europe

[48] https://unfccc.int/fr/a-propos-des-ndcs/l-accord-de-paris Consulted 8 April 2024.

[49] IEA, Transport sector CO2 emissions by mode in the Sustainable Development Scenario, 2000-2030, IEA, Paris https://urlz.fr/qbhP

[50] Batteiger, Valentin et al., (2022). Power-to-Liquids - A scalable and sustainable fuel supply perspective for aviation, https://www.umweltbundesamt.de/sites/default/files/medien/376/publikationen/background_paper_power-to-liquids_aviation_2022.pdf

[51] González-Castaño, Miriam, et al. ■ The Reverse Water Gas Shift Reaction: A Process Systems Engineering Perspective ■. Reaction Chemistry & Engineering, vol. 6, no 6, June 2021, https://doi.org/10.1039/D0RE00478B

[52] ■ Technology Data for Renewable Fuels ■. The Danish Energy Agency, 22 March 2018, https://ens.dk/en/our-services/projections-and-models/technology-data/technology-data-renewable-fuels

[53] König, Daniel H., et al. ■ Simulation and evaluation of a process concept for the generation of synthetic fuel from CO2 and H2 ■. Energy, vol. 91, November 2015, p. 833-41. ScienceDirect, https://doi.org/10.1016/j.energy.2015.08.099

[54] Colelli, Leonardo, et al. ■ E-fuels, technical and economic analysis of the production of synthetic kerosene precursor as sustainable aviation fuel ■. Energy Conversion and Management, vol. 288, juillet 2023, p. 117165. ScienceDirect, https://doi.org/10.1016/j.enconman.2023.117165

[55] Sayed Ahmed, Hassan. Power-to-X: Modelling of Fischer-Tropsch Synthesis in Aspen Plus. January 2022. aaltodoc.aalto.fi, https://aaltodoc.aalto.fi/handle/123456789/112650

[56] Dieterich, Vincent, et al. ■ Power-to-Liquid via Synthesis of Methanol, DME or Fischer–Tropsch-Fuels: A Review ■. Energy & Environmental Science, vol. 13, no 10, 2020, p. 3207-52 , https://doi.org/10.1039/D0EE01187H

[57] Peters, Ralf, et al. ■ A Techno-Economic Assessment of Fischer–Tropsch Fuels Based on Syngas from Co-Electrolysis ■. Processes, vol. 10, no 4, April 2022, https://doi.org/10.3390/pr10040699

[58] Atsonios, Konstantinos, et al. ■ Process analysis and comparative assessment of advanced thermochemical pathways for e-kerosene production ■. Energy, vol. 278, September 2023, p. 127868. ScienceDirect, https://doi.org/10.1016/j.energy.2023.127868

[59] Schubert, Nicolai. 13th International Colloquium Fuels: Conventional and Future Energy for Automobiles. expert verlag, 2021

[60] ElSayed, Mai, et al. ■ Analysing the techno-economic impact of e-fuels and e-chemicals production for exports and carbon dioxide removal on the energy system of sunbelt countries – Case of Egypt ■. Applied Energy, vol. 343, August 2023, p. 121216. ScienceDirect, https://doi.org/10.1016/j.apenergy.2023.121216

[61] Delgado, Hernan E., et al. ■ Techno-economic analysis and life cycle analysis of e-fuel production using nuclear energy ■. Journal of CO2 Utilization, vol. 72, June 2023, p. 102481. ScienceDirect, https://doi.org/10.1016/j.jcou.2023.102481

[62] Pratschner, Simon, et al. ■ Off-Grid vs. Grid-Based: Techno-Economic Assessment of a Power-to-Liquid Plant Combining Solid-Oxide Electrolysis and Fischer-Tropsch Synthesis ■. Chemical Engineering Journal, vol. 481, February 2024, p. 148413., https://doi.org/10.1016/j.cej.2023.148413

[63] Mohebali Nejadian, Mehrnaz, et al. ■ Comparative optimization study of three novel integrated hydrogen production systems with SOEC, PEM, and alkaline electrolyzer ■. Fuel, vol. 336, mars 2023, p. 126835. ScienceDirect, https://doi.org/10.1016/j.fuel.2022.126835

[64] European Center for Medium Range Weather Forecasts (ECMWF) (2020). ERA5 Database, https://www.ecmwf.int/en/forecasts/datasets/reanalysis-datasets/era5

[65] TrinaSolar (2017). TrinaSolar AllMax M Plus Monocrystalline Module Data Sheet, https://www.trinasolar.com/en-apac/resources/downloads

[66] Haas, S., Schachler, B., and Krien, U. (2019). Windpowerlib - A Python Library to Model Wind Power Plants (v0.2.0), https://windpowerlib.readthedocs.io/en/stable/index.html

[67] JRC Photovoltaic Geographical Information System (PVGIS) - European Commission. https://re.jrc.ec.europa.eu/pvg_tools/en/

[68] European Center for Medium Range Weather Forecasts (ECMWF) (2020). ERA5 Database.https://www.ecmwf.int/en/forecasts/datasets/reanalysis-datasets/era5